The relative potential of chemical dissolution driven erosion in limestone bedrock rivers

Georgina Jenkins

The relative potential of chemical dissolution driven erosion in limestone bedrock rivers

Georgina L. Jenkins

MSc by Research

Department of Geography

Durham University

October 2025

Abstract

Identifying how chemical and physical bedrock erosion processes combine is crucial in understanding how upland landscapes evolve through bedrock channel incision. It is well established that abrasion by saltating bedload is a critical process and there is widespread recognition that dissolution of soluble minerals in carbonate bedrock rivers is highly effective, but there has not been work directly quantifying the relative rates of dissolution and abrasion on bedrock incision. Using a combination of laboratory abrasion mill and bedrock cube mass loss experiments, this study assesses the role of dissolution and abrasion across a range of environmental conditions. Laboratory cube experiments were run at three temperature points and three pHs, while field cubes were places at different immersion frequencies in Trout Beck, to see how these factors would affect mass loss. Results showed no difference in mass loss between temperature bands, while pH was a statistically significant indicator of mass loss. The field results showed that immersion time was not the main control on mass loss, with wetting and drying cycles and acidic peat runoff having more control. To compare the contributions of abrasion and dissolution on carbonate rocks, an abrasion mill was used with variable pH solutions, with and without sediment load. In the mill experiments, similar mass loss rates were found for the mill run at pH 7 with bedload (abrasion-driven) and pH 3 with no bedload (dissolution-driven). In addition, the mill experimental runs found evidence that the addition of abrasive tools led to an increase in chemical dissolution rates, while the addition of dissolution did not increase abrasion rates. This study has shown that in low pH carbonate bedrock channels dissolution has the potential to produce similar mass loss as physical processes, challenging the widely accepted paradigm that physical processes are the main control on bedrock channel incision.

Declaration and statement of copyright

I confirm that no part of the material presented in this thesis has previously been submitted by myself or any person, for a degree in this or any other university. In all cases, where it is relevant, material from the work of others has been acknowledged. The copyright of this thesis rests with the author. No quotation from it should be published without prior consent, and information derived from it should be acknowledged.

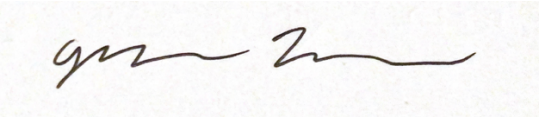

Georgina Jenkins, October 1st, 2025

Contents

List of Figures

and 7 visually to make overlapping points easier to view. The scatter plots also have error bars, showing one standard deviation above and below each data point.

Figure 12: Plots showing the end solution cation levels of the cubes in each 22-hour run depending on (a) average temperature of the run, (b) depending on average temperature, but only at the two higher pHs, and (c) the starting pH of the run. Each dot represents one 22-hour run. The error bars show one standard deviation above and below each data point.

Figure 13: Plots showing the time it took for the solution to buffer from pH 3 to 7. 4a shows the buffer times in a box and whisker plot. The orange line represents the median of the data, the edges of the box show the 25^{th} and 75^{th} percentile, with the whiskers extending out 1.5 times the IQR (difference between the 25^{th} and 75^{th} percentiles). This data had no outliers, or points beyond the whisker range. Each dot represents one 22-hour run.

Figure 14: Mass loss for different cube sizes in (a) percent change, (b)grams and (c)g cm^{-2}

Figure 15: Bar charts showing the proportion of the total mass loss from each 35-hour run that was produced through suspended and dissolved load in (a) percentage and (b) grams

Figure 16: Plot showing the solution cation levels of abrasion mill solution at the end of each 7-hour day.

Figure 17: Bar charts showing the proportion of the total mass loss from each 35-hour run that was produced through suspended and dissolved load in (a) percentage and (b) grams

Figure 18: Plots showing the mass loss of cubes suspended in different sections of Trout Beck for 120 days, with mass loss reported in (a) percent change, (b) grams lost, and (c) grams per cm^2. The orange line in these box and whisker plots represent the median of the data, the edges of the box show the 25^{th} and 75^{th} percentile, with the whiskers extending out 1.5 times the IQR (difference between the 25^{th} and 75^{th} percentiles). The circle in 7b shows an outlier in the data, where it is beyond the whisker range.

Figure 19: Diagram showing the proportion of total mass loss that occurred through dissolved load (D_L) and suspended load (S_L) in abrasion mill experiments run at pH 3, with abrasive beads, for 35 hours

Figure 20: Diagram showing the proportion of total mass loss that occurred through dissolved load (D_L) and suspended load (S_L) in abrasion mill experiments run at pH 3 and pH 7, each with and without

abrasive beads, for 35 hours. All the disks are 1[ce]:1[sa]:1[sh]. pH 3 with beads was run for two sets of 35 hours, the average of these two runs is shown in this diagram.

Figure 21: The characteristic values of tensile strength for limestone and dolomitic rocks (Paronuzzi and Serafini, 2009)

List of Tables

List of equations

$$CO_2(g) + H_2O\ (l) \leftrightarrow H_2CO_3(aq) \leftrightarrow H^+(aq) + HCO_3^-(aq)$$

Equation 1: The creation of carbonic acid, and the carbonic disassociation of H+ protons and creation of the bicarbonate ion

$$CaCO_3(s) + H^+(aq) \rightarrow Ca^{2+}(aq) + HCO_3^-(aq)$$

Equation 2: The dissolution of calcium carbonate (limestone) when attacked by protons, the dominant process at pH 3

$$CaCO_3(s) + H_2CO_3(aq) \rightarrow Ca^{2+} + 2HCO_3^-$$

Equation 3: Dissolution of limestone at pH 7 from interaction with carbonic acid

$$k = Ae^{-E_a/RT}$$

Equation 4: Arrhenius equation relating the activation energy (E_a) to the rate constant (k) and temperature (T) in Kelvin, where A is the pre-exponential factor and R is the gas constant

$$CO_2(aq) + H_2O \leftrightarrow H_2CO_3 \leftrightarrow HCO_3 + H^+ \leftrightarrow CO_3^{2-} + 2H^+$$

Equation 5: The carbonate buffer system that occurs when carbon dioxide (CO_2) dissolves in water (H_2O)

Acknowledgements

Firstly, I would like to thank my supervisors Lizzie Dingle, Jeff Warburton, and Helen Mackay for all of their help at every stage of this research, and for accepting me into such an interesting project. I would also like to thank Aimee-Louise Wilkin, Eleanor Ross, and Robyn Pinder for all of their help in the laboratory. Additionally, thank you to Neil Tunstall and Christopher Longley for their help and for sharing their lab space with me.

Lastly, I would like to thank my family and friends, especially my little brother Hugo and sister Emily, for all of their emotional support over the last year (and beyond).

1. Introduction

The morphology of river channels, and how this relates to their flow and erosional history, is a critical topic in geomorphological research. River incision into bedrock shapes the Earth's topography, driving landscape evolution and coupling changes on the surface to related changes in climate and tectonics in upland environments (Beer and Lamb, 2021). Fluvial systems can also play a large role in sediment transfer, moving materials between upland and lower landscapes (Cook et al., 2012). Extreme discharge events are especially important in longer-term landscape evolution, as larger floods accelerate rates of lateral and vertical bedrock channel erosion (Deal and Botter, 2018; Turowski et al., 2007). As climate change leads to changing spatial and temporal patterns and magnitudes of extreme rainfall-runoff events, understanding the links between fluvial and surface processes such as acid runoff, carbon drawdown and sediment movement systems is becoming even more crucial (Wasko et al., 2021). When considering rivers in limestone terrain or landscapes, research is strongly linked to climate change and rising levels of carbon in the atmosphere. Carbonate rocks make up a critical global carbon store, so it is crucial to understand the exact ways in which the erosion of carbonate landscapes fits into the global carbon cycle (Li et al., 2019).

In recent years, research on fluvial systems has increasingly focused on bedrock and semi-alluvial rivers – fluvial forms where the riverbed does not have substantial alluvial cover and channel form evolves through bedrock erosion, the detachment and removal of bedrock from rock surfaces (Turowski et al., 2008; Spotila et al., 2015; Dai et al., 2021). Bedrock river morphology is highly variable, with variations in width, depth, and curvature linked to physiogeological boundaries, and changes in discharge and bedrock erosion rate (Lamb et al., 2015; Spotila et al., 2015). River bed erosion is thought to be largely driven by physical processes, which cause weakening of bedrock surfaces by internal (e.g. tectonic, topographic, and heating pressures) or external stress (e.g. hydraulic forces from river flow, and abrasion by transported sediments) placed on bedrock surfaces, and chemical processes, (those that cause rock mass loss through chemical alteration of constituent minerals) (Yokoyama and Matsukura, 2006). In limestone bedrock rivers, the main physical and chemical processes are abrasion and plucking, and dissolution (Yokoyama and Matsukura, 2006; Lamb et al., 2015). There is a large body of literature investigating rates and mechanisms of abrasion and plucking, through both field and laboratory work (Beer and Turowski, 2015; Sklar and Dietrich, 2001; Turowski et al., 2007). Chemical dissolution has also been simulated through laboratory work, looking at the rates of dissolution that occur across largely high temperatures, and low pHs (Cahoon et al., 1993, Covington et al., 2015; Hattanji et al., 2014).

Despite the research that has been performed on erosion in bedrock rivers, there is still considerable uncertainty about the relative significance of chemical and physical processes. While spatial patterns of chemical weathering are largely clear, the large uncertainties surrounding chemical weathering in bedrock rivers lies in the comparative rates and magnitudes of chemical and physical erosion. This study simulates relative rates of bedrock chemical weathering and physical erosion in the laboratory using dissolution cube experiments and an abrasion mill, as well as looking at dissolution rates in the field, in order to reduce uncertainties in the importance of chemical processes in fluvial systems. These relationships are particularly important in carbonate landscapes where rocks, like limestone, are more susceptible to dissolution.

2. Literature Review

This section provides an overview of chemical and physical regimes of erosion, in fluvial systems. Physical abrasion is explained first, focusing on controls, and the ways in which these controls have been tested. Then it moves on to chemical weathering, explaining the process by which chemical dissolution occurs, highlighting the limited research in fluvial and cold environment research. The importance of chemical weathering in rivers is discussed, outlying the laboratory and field experiments that have been performed that take dissolution into account, or focus solely on it. Finally, this section discusses the current understanding of controls on dissolution.

2.1 Physical erosion

Physical abrasion of riverbeds is commonly cited as one of the most important factors in river bedrock erosion, with a strong research focus on the different controls on the process (Sklar and Dietrich, 2006). In river channels, rates of physical erosion by abrasion are largely tied to sediment supply, which controls erosion through both the tool and cover effects (Turowski et al., 2007). The tool effect describes the increase in erosion rate with sediment supply, due to increasing particle impacts on the bed, whereas the cover effect describes how sediment supply can shield the riverbed from direct erosion (Sklar and Dietrich, 2001). Field and laboratory work have suggested that maximum abrasion occurs at a sediment load right before the cover effect outweighs the tool effect (Figure 1) (Beer and Turowski, 2015; Sklar and Dietrich, 2001; Turowski et al., 2007). This transition point shifts due to changes in flow conditions (discharge, channel size, spatial variability of velocity over the bed) and bed-material characteristics (the relative protrusion of grains, clustering or packing of particles, grain shape, and grain size distribution) (Knighton, 1998). Transport stage is critical, with field observations suggesting higher erosion rates occur in bedrock rivers where coarse bedload dominates over suspended sediment transport (Smith et al., 1995; Cook et al., 2012). This means that the grain size distribution of the sediment supplied to rivers systems, and from erosional processes within the system, is a fundamental control on bedrock channel development (Sklar and Dietrich, 2001). Erosion in bedrock channels may also occur through plucking (quarrying) of bedrock material, with larger plucked fragments occurring more in rivers with steep stream gradients or frequent flood events causing higher impact energies, which also increases abrasion rates (Howard et al., 1994; Beer and Lamb, 2021; Turowski et al., 2023b).

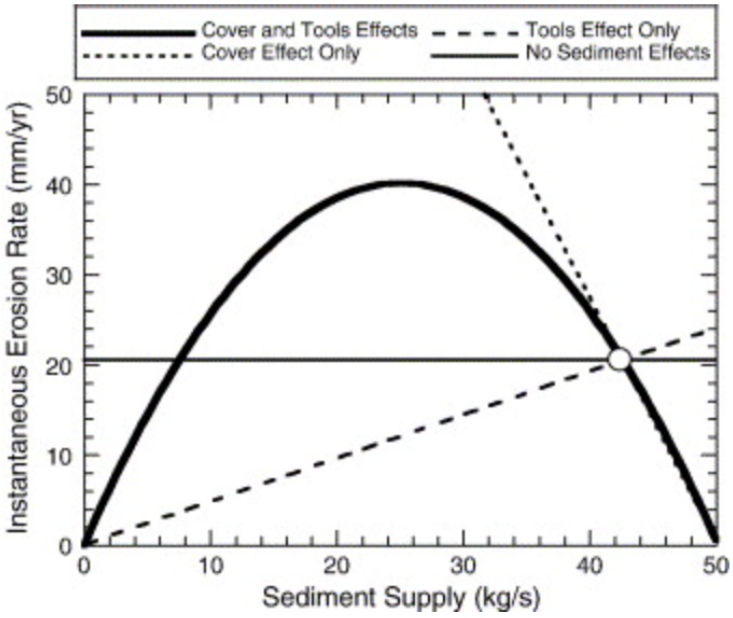

Figure 1: Instantaneous bedrock erosion as a function of sediment supply from four classes of incision models calculated from a mixed bedrock-alluvial river (Sklar and Dietrich, 2006)

In addition to sediment supply, other factors such as flow hydraulics, bedrock composition, and sediment grain characteristics control the physical erosion rates of bedrock rivers (Knighton, 1998; Dubinski and Wohl, 2013; Turowski et al., 2023a). Flow properties such as the magnitude, frequency and variability of stream discharge, velocity, and shear stress influence the rate at which physical breakdown of underlying bedrock material occurs (Knighton, 1998; Lague et al., 2005; Dubinski and Wohl, 2013). Turbulence (shear stress variations) in the river can also have a large impact on localised abrasion patterns at the micro and meso-scales, whereas stream power is more important when looking at a macro scale of channel morphology (Wohl, 1998). Laboratory experiments using a mill apparatus have shown that rock resistance to abrasion scales with the square of rock tensile strength (Sklar and Dietrich, 2001). At a micro-scale, mineralogy, the time that exposed substrate has been on the surface, and local heterogeneities in composition are all key controls on determining the resistance of rocks to fluvial bedrock incision (Wohl, 1998). Sediment grain size is an important control on the abrasion regime because fine sediment will often be suspended, and larger sediment will not be carried by the stream, meaning that both are inefficient erosive materials (Knighton, 1998; Sklar and Dietrich, 2001).

Laboratory simulations are frequently used to investigate how abrasion occurs in natural systems. Sklar and Dietrich (2001) used an abrasion mill to circulate water with varying sediment loads above an erodible bedrock base plate. The experiments demonstrated the tool and cover effects, corroborating field

observations that maximum erosion rates occur at a critical level where bedrock is partially exposed to coarse grained sediment impacts. This experimental setup has subsequently been used to quantify the erodibility for different natural lithologies under fluvial impact erosion (Turowski et al., 2023a). Flume and mill experiments targeting how bedrock properties control channel morphology have shown that rock tensile strength is crucial in controlling bed roughness and abrasion rates (Sklar and Dietrich, 2001; Finnegan et al., 2007; Lamb et al., 2015). These laboratory results, as well as field measurements of physical abrasion, have been used to augment fluvial erosion models, but many lack consideration of chemical dissolution of bedrock (Howard et al., 1994; Davy and Lague, 2009; Beer and Turowski, 2015; Covington et al., 2015; Lamb et al., 2015; Deal and Botter, 2018; Turowski et al., 2023b).

2.2 Chemical dissolution of limestone bedrock

Chemical weathering – the in-situ breakdown of rock material due to chemical reactions – of limestone ($CaCO_3$) largely occurs through dissolution, the process through which a solute dissolves in a solution. In the context of limestone, water dissolves soluble calcium carbonate minerals, primarily calcite. This can occur through carbonation, where CO_2 dissolves in water, creating carbonic acid (H_2CO_3) (Equation 1).

$$CO_2(g) + H_2O\ (l) \leftrightarrow H_2CO_3(aq) \leftrightarrow H^+(aq) + HCO_3^-(aq)$$

Equation 1: The creation of carbonic acid, and the carbonic disassociation of H+ protons and creation of the bicarbonate ion

Limestone dissolution then occurs with the loose protons attacking the bonds in the calcium, releasing calcium cations (Equation 2).

$$CaCO_3(s) + H^+(aq) \rightarrow Ca^{2+}(aq) + HCO_3^-(aq)$$

Equation 2: The dissolution of calcium carbonate (limestone) when attacked by protons, the dominant process at pH 3

At pH 7, limestone dissolution occurs through interaction with carbonic acid, where activation energy is required for the H+ protons to disassociate and react with the limestone (Equation 3).

$$CaCO_3(s) + H_2CO_3(aq) \rightarrow Ca^{2+} + 2HCO_3^-$$

Equation 3: Dissolution of limestone at pH 7 from interaction with carbonic acid

The dissolution of limestone occurs through the calcium constituents being dissolved by the hydrogen protons attacking the rock, splitting off the calcium and reacting with the CO_3 to creation the bicarbonate ion (HCO_3). At low pHs, this process occurs freely, as there is an abundance of hydrogen protons available to start these reactions. At higher pHs, the carbon species transitions from carbonic acid to bicarbonate, which accepts hydrogen ions rather than liberating them while stable. This means that a higher activation energy needs to be met, usually from heating, in order to release the protons to attack the limestone.

The dissolution of rock is largely controlled by factors relating to both the solution that is eroding the rock, and the properties of the rock itself (Briolet et al., 2025). The main factors of the fluid that matter are the chemical composition, pH, flow velocity, and the temperature, while for the rock mineral content, porosity, and permeability are key (Lamarca-Irisarri et al., 2019: Briolet et al., 2025). Low pH values, high temperatures, and high flow values are all related to higher dissolution rates. Temperature has a direct impact on reaction kinetics as temperature controls whether a reaction sustains the activation energy, with diffusion seen to increase with increasing temperature by two orders of magnitude from 0° to 1000°C (Oelkers and Helgeson, 1988; Alkattan et al., 1998). pH however modifies the rate of reaction by affecting the reactivity of minerals, with lower pHs meaning more H+ ions are available to react with the mineral surface, breaking the bonds that hold the constituent rock elements together. Chemical weathering is linked to chemical erosion, the removal of rock material due to chemical reactions, and chemical denudation, which is the long-term reduction of the earth's surface due to chemical erosion. In river systems, erosion and weathering often go hand in hand, as the water that chemically weathers a rock surface is then well poised to remove it, so in this thesis chemical weathering will be used to describe the breakdown and removal of this material.

Research on weathering of the built environment has involved many studies looking at the effects of dissolution on limestone structures, mainly through rain and sea water splash. Such studies have linked physical and chemical weathering, showing that wind driven physical abrasion at a micro level creates grain boundaries at the micron-scale that rapidly increase rain-driven limestone dissolution, which in turn leads to further physical erosion as tiny particles mechanically detach (Emmanuel and Levenson, 2014).

Acidic, low pH, rivers provide conditions for enhanced chemical weathering. Acidic rivers can come from many naturally occurring or man-driven processes (Table 1). Acidic runoff from soils impacted by acid precipitation is a common cause of acidic waterways (Frei et al., 2000). Long-term monitoring of the Niigata and Gifu Prefectures in Japan, from the mid 1980s to early 2000s, showed a negative trend in pH,

from around neutral to an acidic pH of 6, due to acidification from soil runoff (Matsubara et al., 2009). A study looking at 34 springs in the Northern Harz Mountains in Germany, with a dominant granite lithology, showed similar trends, with spring waters reaching pHs as low as 4 (Frei et al., 2000). A study on Lake Usoriko in Japan found that acidic runoff containing sulfuric and hydrochloric acid from volcanic sources had acidified the lake water to between pH 3.4 and 3.8 (Satake et al., 1995). While the sedentary nature of lake water means that it often retains acidic runoff more than river systems, rivers discharging from lakes can be fed by this acidic water (Satake et al., 1995). Vegetation cover can acidify connected groundwater through storage and leaching of CO_2, leading to acidic runoff into fluvial systems. A study examining 26 peatbogs in Pomerania, northwest Poland, showed that runoff from peat-bog environments can reach pHs as low as 3.4 due to concentrated organic carbon buildup in the top peat layer (Banas and Gos, 2004). Low pH rivers can also occur due to human-made contaminants, such as mine drainage. This can occur long after the active period of mining due to the leaching of left-over mine waste (Brake et al., 2001; Gundersen and Steinnes, 2001; Olías et al., 2004). Rivers draining mining regions across the world show low pH levels. pHs between 2.5 and 6.3 have been found in the Odiel River in Spain which drains from an area that has been associated with sulfide mining since prehistoric times (Olías et al., 2004). West Little Sugar Creek in west-central Indiana, USA changes from a slightly alkaline pH range of 7.6-8.6 to under 3.7 past the points of contamination from the Green Valley coal mining site which has not been active since 1963 (Brake et al., 2001). Bedrock geology has been shown to have a strong influence on the pH of rivers through different buffering capabilities, with rivers remaining more acidic in areas where underlying bedrock has a low neutralizing capacity (Frei et al., 2000; Matsubara et al., 2009). This means that acidic rivers have the most chemical weathering potential when moving from a low solubility source or reach, such as granitic, to a more carbonate-rich geology, like limestone (Frei et al., 2000).

Table 1: Field measurements of low pH rivers

Paper	Cause of acidification	Region/Country	Geology	pH
Satake et al. (1995)	Volcanic runoff	Lake Usoriko, Japan	Ash, mudstone, and volcanic breccia	3.4 and 3.8
Frei et al. (2000)	Increased precipitation	Ecker watershed of the Northern Harz Mountains, Germany	Granite	4-6
Brake et al. (2001)	Coal mine site contamination	West Little Sugar Creek in west-central Indiana, USA	___	Under 3.7
Banas and Gos (2004)	Peat-bog runoff	Pomerania, NW Poland	___	Runoff between 3.4 and 3.7
Olías et al. (2004)	Mine site contamination	Odiel River, Spain	Limestone above the mine site, pyritic bedrock through and after the mines	2.5-6.3
Matsubara et al. (2009)	Acid deposition from the atmosphere	Niigata and Gifu prefectures, Japan	Granitic	Declining trend to pH of 6

2.2.1 Laboratory chemical weathering simulations and flow through experiments

Laboratory experiments designed to isolate a single controlling factor are commonly used to investigate specific erosional processes (Table 2). Alkattan et al. (1988)'s experiment rotated a disk of limestone within a stagnant solution, demonstrating that calcite dissolution rates increased at lower pH and higher

temperature. Flow-through experiments with a constant supply of fresh weathering solution have been used by researchers to investigate chemical dissolution of limestone, with higher flow rates linked to increased dissolution, as new water unsaturated in calcite has a higher dissolution potential (Hattanji et al., 2014). Flow-through experiments have the advantage of maintaining a constant pH and avoiding saturation of the test solution, which would inhibit further dissolution. Similar flow through experiments have been performed on limestone tablets to show that increased immersion time in a constant CO_2 solution leads to a shift from carbonic acid weakening to corroding the sample, with CO_2 solution causing a dissolution rate 11.8 times that of deionised water (Dong et al., 2024). However, comparison of dissolution rates from flow-through experiments and an aquifer field site in a small catchment at a forested mountain slope in the Abukuma granitic terrain in northeast Japan, showed laboratory rates to be around 50 times slower than in the field (Yokoyama and Matsukura, 2006). The field mass loss rates were likely higher due to the inclusion of abrasion, which both introduced physical erosion rates, and could have increased the dissolution rates through the positive feedback that Cahoon et al. (1993) found. Laboratory dissolution experiments commonly do not reflect natural conditions, being run at high temperatures (largely > 20°C) or not researching both physical and chemical weathering. Therefore, further research replicating conditions tied to real locations and examining both types of erosion, and how they affect each other is crucial to gain more accurate insight into bedrock channel processes.

2.2.2 Low temperature carbonate dissolution

Before 1960, it was widely accepted that dissolution rates were sensitive to temperature, and that dissolution thus had limited impact in cold environments where lower rates were expected (Rapp, 1960). In 1960, Rapp's work changed this longstanding paradigm that chemical weathering had limited impact in cold environments, finding indicators of past chemical limestone and schist weathering in Kärkevagge, Northern Sweden, a periglacial mountainous environment. The water here is dominated by bicarbonate and sulfate, dissolved from the marble and schist sides of the valley respectively (Campbell et al., 2001). Laboratory dissolution data at low temperatures, and chemical markers of rock weathering reactions in several periglacial locations have shown calcium and sodium dissolution from carbonate and silicate materials is higher at lower temperatures, potentially because cold water dissolves more CO2 (Gaillardet et al., 2019; Hodson et al., 2010). For example, dissolution was the key factor in the creation of weathering rinds in the Hallstatter Glacier in the Dachstein Mountains, Austria, and was shown to be more effective following fracturing of the bedrock (Dabski et al., 2019). Increased physical weathering from freeze-thaw processes in cold environments leads to rock fatigue, providing weaker material for chemical weathering processes meaning that chemical denudation rates in alpine areas exceed the global mean rate (Hoch and Drever, 1999; Dabski et al., 2019). Despite this work, many geomorphologists still

operate under the mis-placed assumption that mechanical rock breakdown dominates, especially in cold environments, and partly consequently studies on the specific nature and intensity of chemical weathering in arctic and alpine environments (and river systems) remain sparse (Gaillardet et al., 2019). Lack of recognition of the importance of cold system chemical weathering and erosion of rock is evident in the fluvial realm, where projects looking at the chemical weathering of limestone and other high solubility rocks tend to focus on temperatures at 20°C and higher (Table 2). As many river systems globally function at lower temperatures, there is uncertainty on how chemical weathering affects these fluvial systems.

2.3 Importance of dissolution in river channels

The relative importance of chemical and physical erosion of riverbeds has not been widely studied (Hattanji et al., 2014; Beer and Turowski, 2015). Models of bedrock channel evolution often presuppose negligible chemical weathering, but this cannot be automatically assumed, especially with soluble carbonate bedrock. Studies of dissolved river load have found that chemical weathering rates were 10 times higher for carbonate than silicate rocks and that carbonate rocks had a higher rate of chemical weathering than 70% of other rock types examined, including granite, gneiss, schist, and sandstone (Covington et al., 2015; Han et al., 2010; Meybeck, 1987). The susceptibility of limestone to chemical dissolution was shown in a nationwide geological survey of Japan where the spatial distribution of calcite clastics in stream sediments from limestone reaches were 50% lower than expected due to dissolution loss of material (Ohta and Minami, 2013).

More recently several studies have sought to quantify the importance of chemical weathering in bedrock rivers. A study looking at US Geological Survey data – alkalinity, temperature, pH, and calcium and magnesium concentrations – showed that calcite dissolution rates from 77 streams were 1- 2 orders of magnitude higher than previous estimates, with carbonate dissolution rate variability between sites controlled by the amount of CO_2 dissolved in water (Covington et al., 2015; Panigraphy and Raymahashay, 2005). Studies using weight loss of limestone tablets, and calcium cation changes across a river reach, across 77 rivers in the continental USA and a limestone plateau in the Abukuma Mountains in Japan have shown that higher discharges and lower calcium concentrations at headwaters of limestone-dominated catchments correlate to high limestone dissolution rates (Covington et al., 2015; Hattanji et al., 2014) (Table 3).

Connections have been found between physical and chemical weathering rates. The long-term study by Riebe et al. (2004) looking at granitic landscapes across diverse climatic conditions found that high

chemical weathering rates correlated with rapid denudation rates, as chemical breakdown increased mineral supply ready to be physically eroded. Cahoon et al. (1993) performed a study looking at chemical weathering of Lake Waccamaw observing limestone tablets submerged in a lake. Their results led them to hypothesise that physical weathering increases rates of chemical weathering by increasing the exposure of fresh rock surfaces (Cahoon et al., 1993). This suggests a positive feedback, showing the co-dependency of physical and chemical rates.

Table 2: Studies of chemical dissolution in laboratory simulations

Paper	**pH range**	**Temperature Range (°C)**	**Rock type**	**What was measured?**	**Flow through/constant acid supply**	**Rates found**
Alkattan et al. (1998)	-1 to 3 (from HCl)	25, 50, 80	Single calcite crystals, limestones, compressed calcite powders	Mass Loss	No	0.07±0.02 to 0.25±0.02 mol $m^{-2}s^{-1}$ from 25° to 80°C
Yokoyama and Matsukura (2006)	Between 6 and 7	20	Granodiorite	Mass loss	Yes	0.0078 to 0.010 wt% yr^{-1}
Sun et al. (2007)	5.2-5.8 (from HCl)	45-60	Limestone slurry	Dissolution rate based on slurry and HCl supply	Yes	—
Thornbush	4.73 vs 6.43	19	Weathered	Ca^{2+} concentration in	Yes	Greater dissolution rates in the

and Viles (2007)	(from H_2CO_3)		and unweathered limestone	water samples		lower pH solution
Hattanji et al. (2014)	No pH change, flow rate changes between 100mL d^{-1} and 4500mL d^{-1}	20	Limestone	Ca ions for input and output solutions	n/a	0.037±0.002 at 100mL d^{-1} and 0.124±0.007 mg $cm^{-2}d^{-1}$ at 4500mL d^{-1}
Dong et al. (2024)	4.2 (from CO2 solution) vs deionized water	Room temperature	Limestone	Ca^{2+} ion changes Dissolution rate	Yes	0.0858 to 3.9602 mg L^{-1} d^{-1} 0.61 to 6.82 wt%
Briolet et al (2025)	Circum-neutral pH	5-26	Micritic limestone	Dissolution rate	Yes	2.42×10^{-07} to 10.88×10^{-07} mol m^{-2} s^{-1}

Table 3: Field estimates of mass loss of rock tablets in river systems

Paper	Rock type	Climatic setting	Placement	What was measured?	Rates found
Hattanji et al. (2014)	Limestone	Humid temperate region, temperatures between -0.9-22.9°C	2 allogeneic streams flowing from non-limestone sources, and one karst spring source, over three years	Weight loss	In allogeneic streams: 0.11-0.14 mg cm^{-2} d^{-1} 0.05 mg cm^{-2} d^{-1} In karst source stream: 0.005 mg cm^{-2} d^{-1} Total: 0.23-4.47g yr^{-1}
Yokoyama and Matsukura (2006)	Granodiorite	—	In and above an aquifer, over ten years	Weight loss - percentage	0.013wt% yr^{-1} above the aquifer, 0.42 wt% yr^{-1} in the aquifer
Krklec et al. (2024)	Limestone and breccia	Mean annual temperature 4.7°C, 5 months with mean monthly temperatures below 0°C	In an open slope, small clearing, and bottom of a doline – in order from least to most precipitation (2172.3 mm of precipitation averaged across area over 372 days), not in a river channel	Average weathering rate (%) | Average denudation rate (μm yr^{-1}) (listed in the same order as the positions in the	Jurassic limestone: 0.149, 0.160, 0.502% | 1.42652, 1.48098, 4.84556 μm yr^{-1} Pg-Ng carb. breccia: 0.146, 0.164, 0.597% | 1.40932, 1.65825, 5.60321 μm yr^{-1}

				previous column)	
Cahoon et al. (1993)	Limestone	Lower pH stream water (6.4) compared to higher pH lake water (7.05)	In a creek mouth versus by the limestone wall in the lake the creek runs into, over 108 days	Mass loss percentage and average rate	<u>In the creek mouth:</u> 9.59% (6.37 g yr^{-1}) <u>In the lake:</u> 3.56% (2.29 g yr^{-1}) <u>limestone -sandstone vs limestone tablets:</u> 4.31 vs 5.82%

3. Study Aim and Hypotheses

This project examines the contribution of chemical processes in overall rates of erosion in limestone bedrock fluvial systems, through the simulation of relative rates of bedrock chemical weathering and physical erosion in laboratory and fieldwork settings, to build a more holistic understanding of limestone channel evolution. Few studies have focused on quantifying rates of chemical weathering in river channels. This has left uncertainty in the relative magnitudes of chemical versus physical processes in bedrock rivers, which this study aims to address through laboratory and field work focusing on limestone and synthetic carbonate bedrock. This will be done specifically through answering the following research questions:

1. What environmental factors (pH, temperature, immersion time) control the dissolution rates of limestone in laboratory cube experiments and river channel field tests?
2. How does rock composition affect synthetic carbonate bedrock dissolution rates in a laboratory setting?
3. What are the relative contributions of physical and chemical processes to overall erosion rates of carbonate bedrock in laboratory abrasion mill experiments?

To answer these research questions, field and laboratory changes in mass of limestone cubes exposed to different environmental conditions were measured. In the laboratory calcium cation concentrations in the end solutions were also measured to provide an additional method for comparing the rates and strength of dissolution occurring in each experimental run. As limestone is largely monomineralic, it is well suited for comparisons of field and laboratory-derived rates of chemical weathering as the same mineral (calcium) is being targeted across both types of experiment (Trudgill and Viles, 1998). Mass loss and calcium concentration of end solutions was also measured for concrete disks exposed to different combinations of acidic and neutral solution, with and without abrasive material in an abrasion mill. Through replicating field conditions in a laboratory setting (as far as is possible) and comparing these laboratory results to those measured in the river sites, this research will provide a clearer picture of limestone dissolution in a realistic fluvial context.

3.1 What environmental factors (pH, temperature, immersion time) control the dissolution rates of limestone in laboratory cube experiments and river channel field tests?

Given the temperature range of the cube experiments (3°-30°C) is less than in previous studies (up to 100°C), pH will likely have a proportionally bigger impact on dissolution rates (Oelkers and Helgeson,

1988; Alkattan et al., 1998). Additionally, as research looking at chemical processes in cold environments has shown that dissolution can have a large impact on rock breakdown in environments around 0°C, the lower end of the experimental temperature range is likely to still show significant chemical dissolution. In the field experiments, the immersion time will have a large control on dissolution rates, with the blocks with the highest immersion times undergoing the most mass loss as they have increased time to undergo dissolution. However, wetting-drying cycles may prove to be an important process, causing the periodically submerged blocks to undergo significant weight loss as these cycles will make them more susceptible to erosive processes.

3.2 How does rock composition affect carbonate bedrock dissolution rates in a laboratory setting?

Higher calcium content will likely be the main control on carbonate bedrock erosion in the abrasion mill. Carbonate rocks have been shown to have chemical dissolution rates over 10 times those of more dissolution resistant rocks like silicate rocks, in both fluvial and out-of-channel contexts. The abrasive material in the mill will work to loosen material to be dissolved, constantly exposing a fresh layer of bedrock. This means that the speed at which this material is dissolved will be partly dependent on how much of each fresh surface is prone to dissolution, or for carbonate rocks how much of each fresh surface is calcium (e.g. the soluble component of limestone in Equations 2 and 3).

3.3 What are the relative contributions of physical and chemical processes to overall erosion rates of carbonate bedrock in laboratory abrasion mill experiments?

In laboratory simulations of carbonate bedrock river erosion, it is hypothesized that chemical processes will be of a similar magnitude to physical erosion processes, especially at the lower pHs. Outside of the fluvial field of research where physical erosion processes are often less effective, chemical dissolution of limestone has long been seen as a dominant control on weathering rates of limestone-built structures. Both laboratory- and field-based research show that mass loss of limestone in fluvial contexts is higher than just abrasion would account for. This suggests that chemical weathering is likely an important process in fluvial systems that has thus been largely unaccounted for. Through the comparison of fieldwork that looks at both chemical and physical erosion, and laboratory-work that isolates the processes from one another, this study will likely find that chemical weathering makes up a larger proportion of bedrock erosion in fluvial systems than previously thought. It is also likely that chemical dissolution will increase physical erosion rates, where the dissolution of soluble elements in the rock will leave insoluble constituents more susceptible to detachment by particle impacts.

4. Methodology

In order to address the main research aim, a combination of laboratory experiments and field observations have been undertaken to quantify the relative role of chemical dissolution in the erosion of limestone bedrock river channels.

4.1 Fieldwork

4.1.1 Field site description

The field site is Rough Sike and Trout Beck rivers in the upper Tees catchment in the Moor House and Upper Teesdale National Nature Reserve, North Pennines (Figure 2 and Table 4). These sites were selected as there is a well-established field monitoring programme in the catchment, providing long-term records of river stream temperature, pH, and local weather used to inform the laboratory experimental setup. In addition, the portion of Trout Beck that encompassed the study site is underlain by limestone, making it suitable for studying erosion of carbonate channels. The research area is characterised by extensive, almost continuous, blanket peat coverage, with few natural exposure sites of bedrock (Johnson, 1963). This vegetative coverage, combined with a high average annual rainfall of 2065 mm, means that there is an abundance of acidic runoff into Trout Beck and Rough Sike rivers, giving minimum and average pH values of 5.9/6.8 and 4.7/5.4 respectively (Table 4, Rennie et al., 2017; Dingle et al., 2025). Situated in the North of England (gauging station with a grid reference of NY757335, latitude of 49.770309), the yearly average air temperature is 6.3°C, with a median stream temperature of 8°C (Table 4).

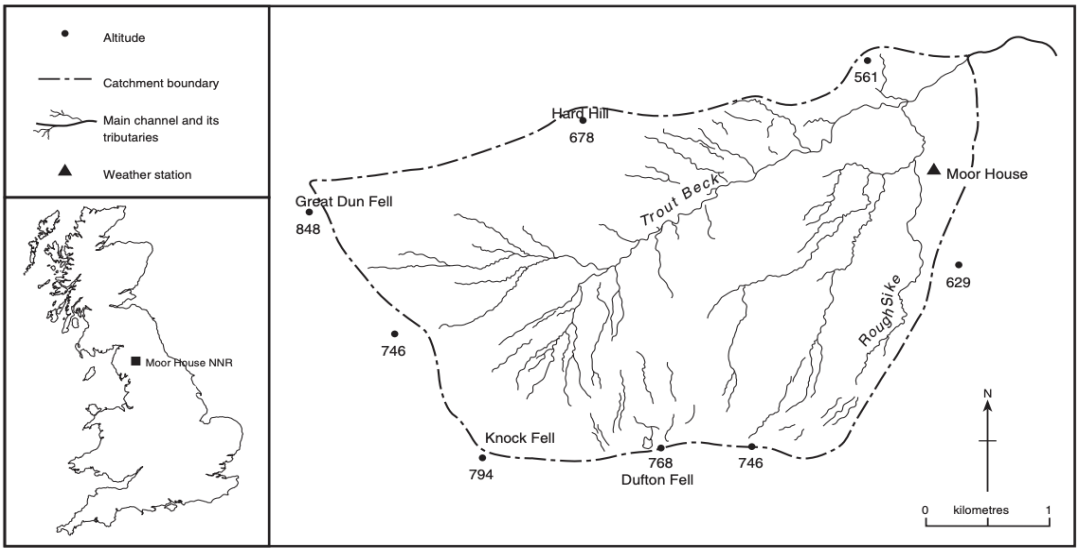

Figure 2: Map of the field site, including both Trout Beck and Rough Sike (adapted from Warburton and Evans, 2011)

Table 4: Site details Trout Beck and Rough Sike (Sharma, 2016; Warburton and Evans, 2011)

Catchment attribute / measurement	**Trout Beck values**	**Rough Sike values**
Yearly air temperature range (1991-2011)	-1.5-15.5°C for the area encompassing both catchments	
Yearly average temperature (1991-2011)	6.3°C for the area encompassing both catchments	
Yearly average rainfall (1991-2012)	2065mm over an average of 240 days for the area encompassing both catchments	
Rough Sike Catchment area	11.4 km^2	0.83 km^2
Lithology of the catchments	Carboniferous series composed of interbedded sandstone, shale, and limestone	
pH of the water	Min: 5.38 Max: 8.14 Median: 6.715 SD: 0.54	Min: 4.74 Max: 7.11 Median: 5.91 SD: 0.59
Water temperature	Min: -0.9°C Max: 24.7°C Median: 8°C SD: 5.9°C	
Land cover	Continuous blanket peat coverage for the area encompassing both catchments	

The lithology of the Moor House and Upper Teesdale National Nature Reserve is largely characterised by several different sub-lithologies of limestone, extensively covered by peat and drift cover, apart from in some of the stream sections where outcrops are found. Along Trout Beck, the limestone is Tyne Bottom and Scar Limestone, well exposed along several stretches of the river (Johnson, 1963). There are also persistent features of Six Fathom Hazle sandstone towards the south of Trout Beck, becoming more rare

downstream to the North (Johnson, 1963; Table 4). Low grade metamorphic shale is found below much of the Tyne Bottom Limestone at Trout Beck Wear. Rough Sike also shows patches of exposed Tyne Bottom Limestone down its reach. In the section of river where the field work occurred, in the spot marked on Figure 3, the bedrock lithology is limestone.

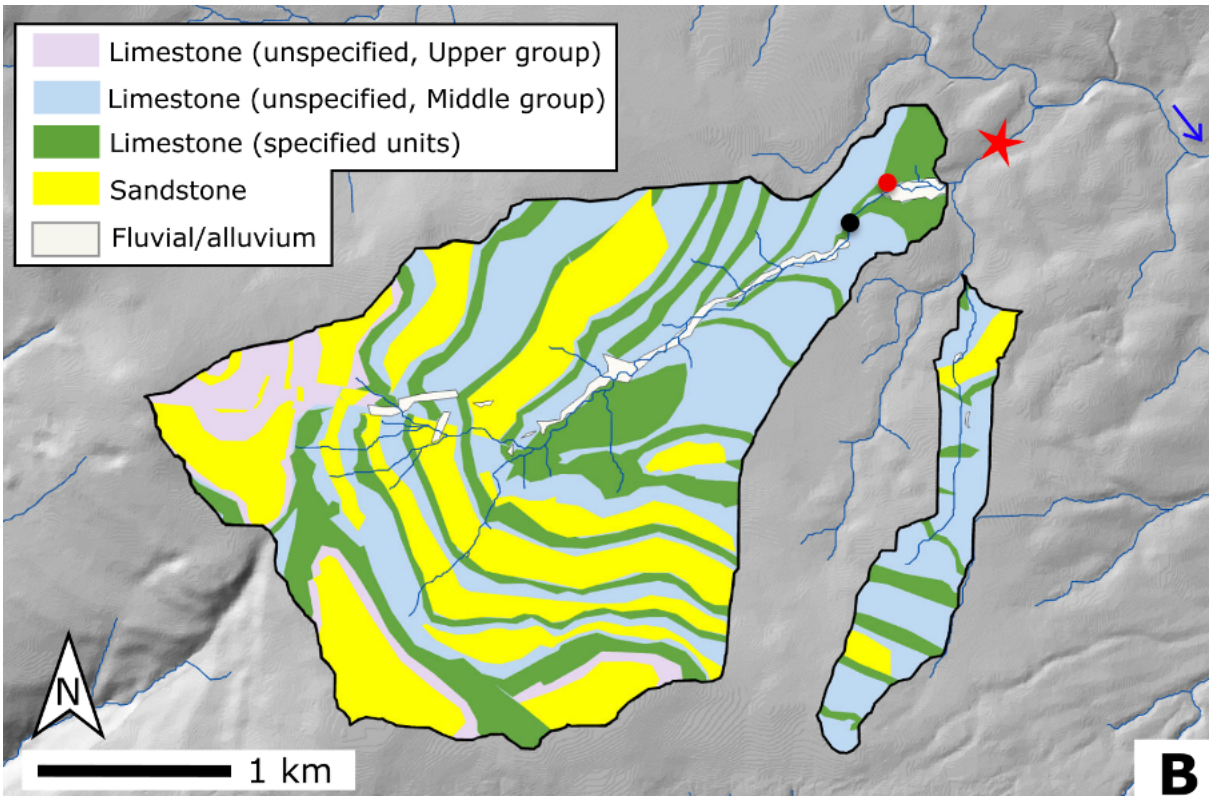

Figure 3: Map of key lithologies of the area, taken from Dingle et al., 2025. The star shows the location of the NRFA gauging station where discharge data is taken. The black circle shows the approximate location of the suspended cubes placed in Trout Beck. The red circle shows the approximate location where the limestone cubes were cut from (for the field and laboratory experiments).

4.1.2 Fieldwork methods used

The use of rock tablets is one of the most common methodologies in field and laboratory-work to calculate denudation rates and spatial distribution of weathering (Alkattan et al., 1988; Hattanji and Matsukura, 2017; Dong et al., 2024; Krklec et al., 2024). Weight loss was measured from blocks of limestone and sandstone (for comparison with a non-carbonate lithology) that had been fixed for four months (7th March 2025 - 4th July 2025) at different heights above the channel, under different flow submergence conditions, looking at how relative rates of erosion differ by channel position and rock tablet composition (Figure 4). The pool cubes were 5 cm from the bed of the channel, while the bench

ones were 20 cm above the bed level, and the bank/atmosphere cubes were approximately 4 m from the bed floor, only exposed to rain and wind, not channel flow. Discharge data was taken from the National River Flow Archive (NRFA) Troutbeck gauging station (station number 25003) to determine the frequency of inundation for each set of cubes. The cubes were places along a cross section taken from Dingle et al. (2025) where the stage discharge relationships have previously been estimated. Discharge data was scaled, following the methodology of Dingle et al. (2025) to account for the gauging station incorporating other tributaries (Figures 7 and 9). This field work, performed in a river with similar solution temperatures to the laboratory experiments, as well as solution pH aligned with some of the laboratory runs, provides a point of comparison for the laboratory work, exploring how the more controlled processes occur in less predictable conditions.

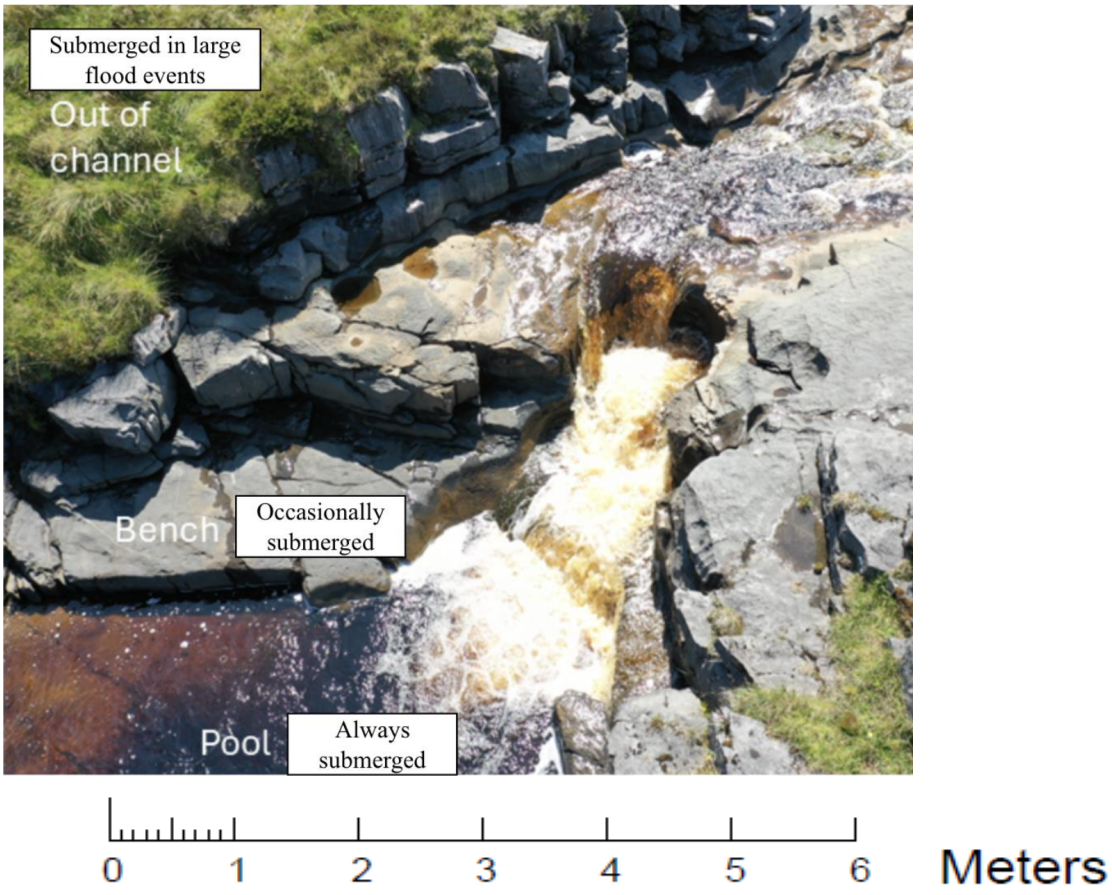

Figure 4: Cross sectional view of how the blocks were attached in Trout Beck

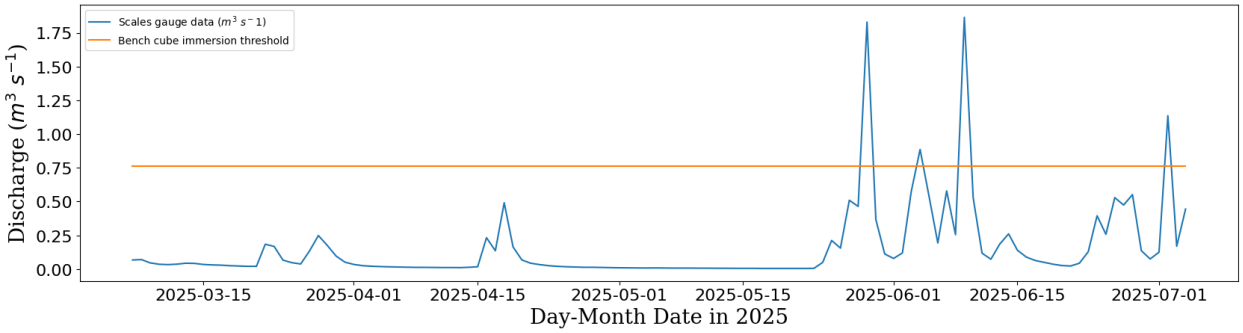

Figure 5: Stage-discharge time series for the study period with lines showing the point of submersion for the pool and bench cubes

4.2 Laboratory cube dissolution experiments

Limestone cubes (of 3, 4, and 5 cm), cut from field site limestone bedrock, were suspended inside 1 L beakers of solution, ranging in pH from 3 to 7 for 22 hours, with four repetitions (Figure 6). This range in pH encompasses the majority of values observed at the two field sites, going lower to incorporate more acidic fluvial channels found across the globe (Tables 1 and 4). For the duration of the experiments, beakers were placed on magnetic hot plate stirrers, to ensure constant mixing of the immersion solution. Experiments were run at 3°C, 17°C, and 30°C. These temperatures were chosen based on monitoring data from the field site which showed a minimum water temperature of -0.9°, an average of 8.3°C, and a high of 24.7°C (Rennie et al., 2017). One set of experiments was run at 17°C as this was the room temperature in the laboratory, and the other two sets were run at 3°C and 30°C to cover the range seen at the field site. This also fits within the use range of the Stuart SD 300 stirrer hot plate. These chosen temperatures showed how limestone dissolution occurs across a realistic temperature range for a northern UK river. The lowest temperature, performed in a cold store, aimed to capture the importance of carbonate chemical weathering observed in cold (periglacial) environments (Gaillardet et al., 2019; Hodson et al., 2010). Table 5shows the experimental setup combinations that were run for this experiment. Each setup that was run had four separate 22 hour runs performed. 22 hours was chosen as it allowed for an entire experimental combination to occur over one week, with 2 hours between each run for solutions to reach the required temperature. The same cube was used for each of the 4 runs at the same combination, giving an overall mass loss for the 88 hours of run time.

Table 5: Matrix of experimental design. Each green box is a combination of temperature, pH, and cube size that was tested with four 22-hour runs (88 hours total)

Cube size	3°C			17°C			30°C		
	pH3	pH5	pH7	pH3	pH5	pH7	pH3	pH5	pH7
3 cm				X					
4 cm	X	X	X	X	X	X	X	X	X
5 cm				X					

A set of experiments was undertaken to look at the effect of sample surface area on dissolution rates, running at room temperature (17°C) and pH 3 with cubes of 3, 4, and 5 cm lengths (see Table 5). These were run for four periods of 22 hours, as with the others. All the other pH and temperature combinations were run with cubes of a side length of 4 cm.

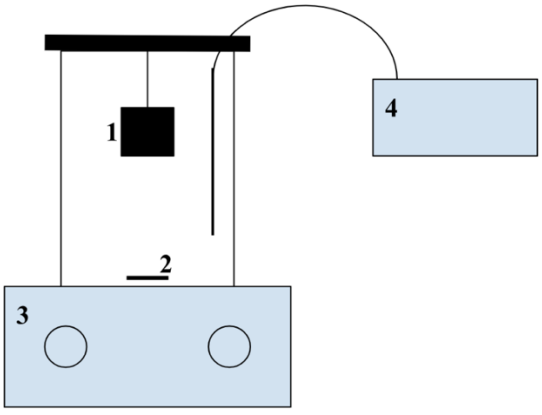

1: Test limestone block, suspended by fishing wire from a rod
2: Magnetic stirrer
3: Magnetic hotplate and stirrer with controls for temperature and stir speed
4: pH, electroconductivity and temperature probes

(a)

(b)

Figure 6: (a) schematic of the experimental set up for the cube experiments (b) photograph of the laboratory set up

4.2.1 General cube experimental procedure

Before the limestone cubes were submerged in beakers, their initial saturated and dry weights were recorded. To take saturated mass, the cubes were soaked for 24 hours in beakers of deionised water. They were then taken out of the beaker one at a time, patted once on each face with paper towels, and then placed on an analytical balance (Sartorius CP225D) for 60 seconds before being weighed to the nearest 0.0001 g. This was repeated three times for each cube, with one minute in water between each measurement, to take an average weight to the nearest 0.0001 g. The cubes were then placed on a labeled metal tray and dried in a 40°C oven for one week. The largest cube was taken out and weighed, placed

back in for an hour, and weighed again to make sure the mass was stable, ensuring the cubes were fully dried out.

The pH solutions were mixed using 10% HCl, which was added into beakers of deionised water through a pipette. Once the beaker contained 900 mL of solution at the intended pH, a plastic rod and nylon fishing string was used to suspend the cube in the beaker, completely covered by the solution. The beakers were placed on electronic magnetic hot plates, with magnetic stirrers in the beakers to keep water flowing throughout the experiment. Once suspended, the cube was left in the solution for 22 hours. After this the cubes were rinsed off and saturated weight was taken in the manner described above before they were resuspended over a new solution of the same pH. A Campbell CR10X data logger was used to measure the pH (Jenway 3510 standard digital pH meter with an 'Environmental Express' probe, accuracy of ± 0.003pH) and temperature (Campbell 107 thermistor, accuracy of ± 0.18°C) of the solution, every 15 minutes through the 22-hour period, to see buffering rates and consistency of temperature. For each acidic run, the time that it took the solution to buffer from pH 3 or 5 to pH 7 was timed. The cubes were soaked for a total of four periods of 22 hours, before final saturated and dry weights were taken.

This gave two sets of mass loss data. Overall mass loss across the 88 hours (4 x 22-hour periods) was measured by both dry and saturated weights, while daily 22-hour mass loss was just measured through saturated weights.

Solution samples were also taken at the end of each 22-hour run to perform UV-visible spectroscopy cation chromatology analysis on. This was performed on the DIONEX-ICS6000 instrument, through isocratic external water suppression with calcium detection limits of 0.04 mg L^{-1}, and with a confidence level of 95%. This allowed for the dissolved amount of calcium to be quantified at each combination.

As these experiments did not include a flow-through element, the solutions that the cubes were submerged in saturated over time. This makes the relation between pH and mass loss less clear than work performed with a flow-through apparatus. Buffer times measured as detailed above will be compared across different runs through the pH logger. This will allow for comparison of buffer times at different temperatures, to extrapolate how indicative the averaged mass loss rates are for each point in time across the run.

4.2.2 Acidic solution preparation

The pH 3 and 5 solutions were made from adding 10% HCl to 900mL of deionised water. The 10% HCl solution was mixed v/v – 100 mL of concentrated 37% HCl in 1L total volume using the HCl bottle dispenser. Measurements during the mixing of solution were done with a Jenway 3510 standard digital pH meter with an 'Environmental Express' probe. The probe was calibrated to three points: pH 4, 7, and 10. This calibration included temperature compensation. Using this probe, 4 mL of stock solution was required to reach pH 3, and 0.1 mL to make pH 5. Cube solutions were mixed based on pH meter readings, as opposed to theoretical measurements from mathematical deductions. After this initial measurement, these quantities were used to mix every batch to ensure comparability across runs, reproducing the same pH value each time.

4.3 Abrasion mill experiments

The abrasion mill (Figure 7), adapted from Turowski et al. (2023), is used here in a novel way to allow for comparison of chemical and physical erosion rates of synthetic bedrock disks. In the past, this experimental design has been used to investigate physical abrasion – looking at tool and cover effect, and how abrasion differs across various lithologies (Turowski et al., 2023a). Abrasion is triggered by the addition of 6 mm diameter borosilicate beads, acting as spherical abraders added into the chamber, and entrained by the turbulent flow created by a rotating motor.

(a) 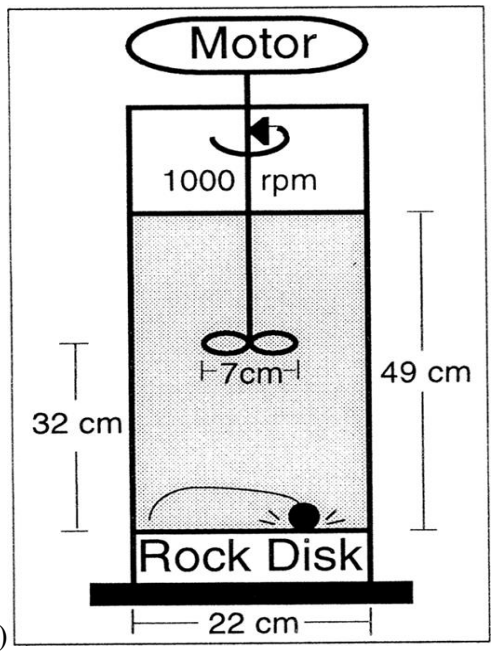

(b) 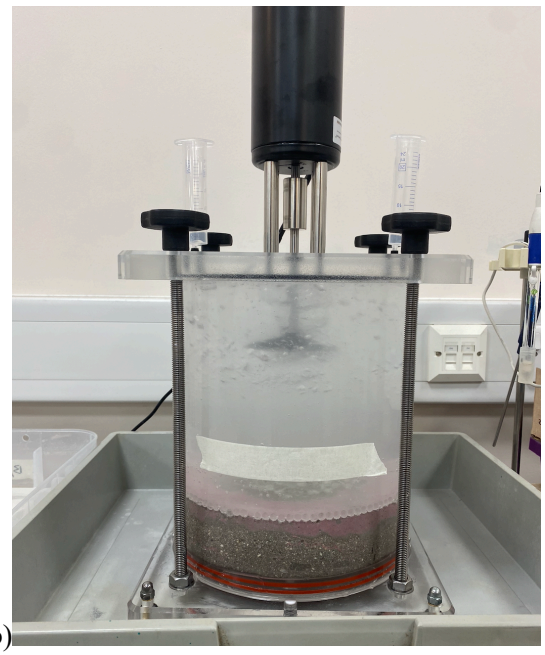

Figure 7 (a) Original design for the abrasion mill (Sklar and Dietrich, 2001), and (b) the abrasion mill in use

In this project, the original experimental design (Figure 7) has been adapted to include differing pH solutions alongside the borosilicate abrasive load, to determine the difference between chemical and physical erosion rates, on synthetic bedrock disks made of carbonate concrete. These disks were tested for both mineral composition and tensile strength to ensure comparability between disks. These abrasion mill experiments were ran at pH 3 and 7, excluding pH 5, as the results from the cube experiments showed that there was no significant difference in cube mass loss between pH 5 and pH 7 (t-test p-value>0.25), showing that a threshold pH value for higher rates of dissolution fell between 3 and 5. In addition, the mill was used to determine the effect of carbonate composition on chemical weathering rates, by varying the composition of the molded concrete bed discs (Table 6). Concrete has been used as an effective bedrock simulant before in experiments looking to isolate tensile strength as a factor in dry abrasion regimes (Beer and Lamb, 2021). In this project, different mixes of concrete are used to isolate carbonate composition and makeup, alongside tensile strength, to demonstrate how site specific or widely applicable results from one carbonate lithology are.

Table 6: Matrix of experimental design for the abrasion mill. Each green box is a combination of pH, abrasive load, and disk composition that was tested with a 35-hour run. The disk composition column shows the ratio (by volume) in each disk mix between cement (ce), sand (sa), and shell (sh).

Disk composition	pH 3		pH 7	
	Beads	No Beads	Beads	No Beads
1[ce]:1[sa]:1[sh]	X	X	X	X
1[ce]:2[sa]	X			
1[ce]:2[sh]	X			

For all the runs, molded concrete disks with an average thickness of 44.4 mm (median: 46.05, standard deviation: 3.55) were used to simulate bedrock in the abrasion mill so that the composition of the bedrock could be varied precisely, and due to ease of replicability and increased homogeneity between duplicate runs. For the runs comparing different pH and bedload compositions, a mixture of 1-1-1 volume ratio between Portland Cement, sand, and crushed shells was used, with a tensile strength of 3.21 (Table 7). For the runs comparing mass loss rates at different compositions, 1-2-0 and 1-0-2 ratios of the above materials were used. Beyond this section these disk compositions will be referred to as 1[ce]:1[sa]:1[sh], 1[ce]:2[sa] and 1[ce]:2[sh], where ce refers to cement, sa to sand, and sh to shell.

Table 7: Summary table for the characteristics of the three disk mixes

Disk composition	Tensile strength	Calcium content from pXRF
1 cement : 1 sand : 1 old shell	3.21 ± 0.29	260,891 ± 2,204
1 cement : 2 sand	2.10 ± 0.20	251,177 ± 2,087
1 cement : 2 new shell	3.82 ± 0.55	345,733 ± 2,719

The tensile strength of the disks at each disk compositions for the abrasion mill experiments were tested indirectly through the 'Splitting' or 'Brazil' test. Disk-shaped rock samples of thickness 25 mm and diameter 70 mm (0.36 T/D ratio) were tested in a Shimadzu AGSX Universal Testing Machine (UTM) equipped with a 300kN load cell (Figure 8). Samples were clamped between two steel loading jaws (platens), and a loading rate of 110 N/s was applied until failure by splitting along the vertical dimeter occurs. The test was run through the Trapezium X Software and results of each test written to a .csv file.

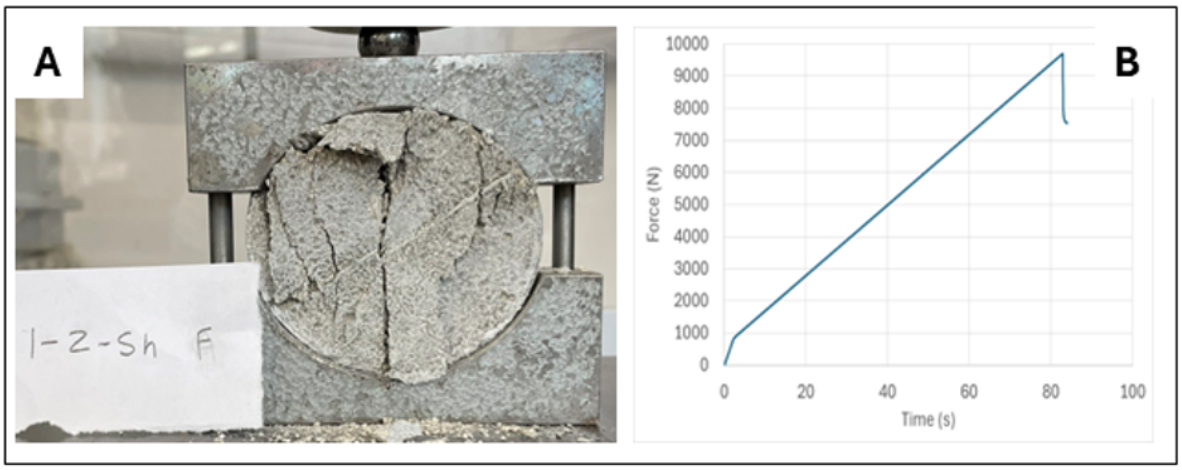

Figure 8: (A) Tensile stress failure of sample TS_1-2-Sh_F. Note vertical tension crack in the centre of the sample. (B) Force to failure graph over time – the step-drop is the point of tensile failure

The grain-size of the components used to make the abrasion mill bedrock disks were all measured using a combination of sieves and a Beckman Coulter LS13320 particle size analyser and analysed for calcium content through portable XRF niton (Figure 9). For the mixes, two different shells were used, referred to in this section as old shell and new shell. This was due to a change in suppliers during the project, but both were composed of crushed shells, with the grain size and calcium concentration detailed below. The sand and old shell (used for the 1[ce]:1[sa]:1[sh] disks) were both 100% under 2 mm. The sand had a median grain size of 308.126 µm, with a standard deviation of 133.39, and a calcium concentration of 1042.07 ± 170.92 ppm. The old shell had a median grain size of 587.896 µm, with a standard deviation of

437.635 and a calcium content of 340617.3 ± 2712.39 ppm. The new shell material (used for the 1[ce]:2[sh] disks) had a median grain size between 500 µm and 1 mm, with a calcium content of 370254.3 ± 2746.45 ppm, around 9% higher than the other shell material.

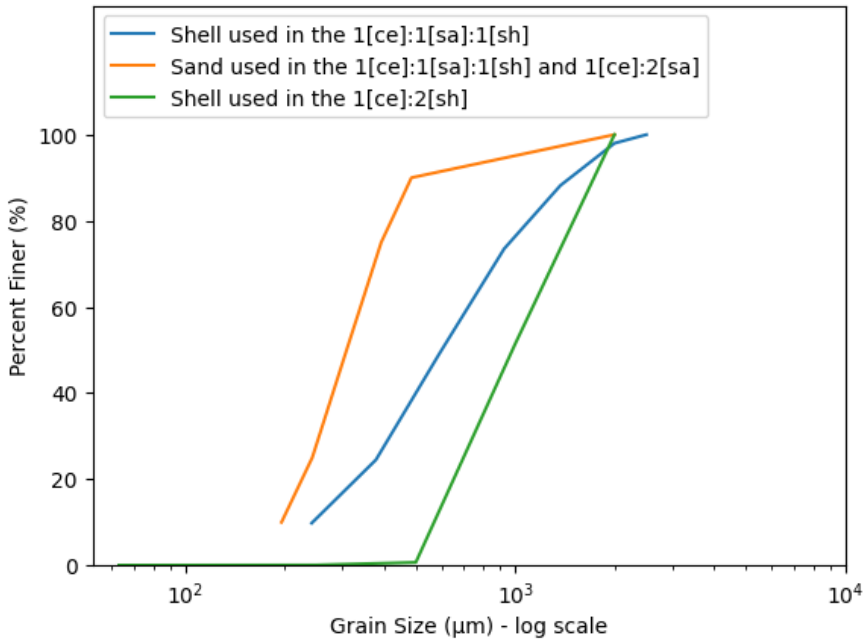

Figure 9: Grain size distribution curve for the sand, and both shell materials used to make the disks

4.3.1 Abrasion mill set up, run time, and dismantling procedure

The concrete disks were set in silicone molds of a diameter of 20 cm and cured for a week in a 40°C drying oven. After this, a dry weight was taken to the nearest hundredth gram (on the Sartorius CP3202S analytical scales), either directly out of the oven or after a redrying period of 48 hours in the oven, and the disks were soaked in a tray of deionized water for a week prior to the experimental run.

Disks were then taken from the water, and each side was patted dry and then sat on the scale for a minute to take a saturated weight. They were then resubmerged for 5 minutes, and this process was repeated twice to get an average saturated weight – the increase in time from the cube procedure reflects the additional time it takes for an object of larger volume to fully saturate. Electronic calipers were used to take 8 depth measurements equidistant around the circumference, to the nearest 0.1 mm.

The disks were then placed on the base of the mill, and the mill chamber was fit around them, pushed down until it was flush with the lower base. Silicone grease was used to ensure a watertight fit. Once in the mill, disks were submerged with deionized water and left for 48 hours to ensure any saturation lost

during the weighing period was regained. This water was then siphoned out and replaced by a 7 L mixture of deionized water and a premixed HCl solution calculated to bring the overall pH of the mill solution to the intended level. As with the cube experiments detailed above (section 4.1.2), HCl was added to deionised water until the Jenway pH probe interface showed the correct pH of 3, and pure deionised water was used for pH 7 runs. The mill has a water-tight seal through four screw-on washer-handle sets and can be topped up with syringes via the portholes on the lid to ensure complete fullness. Open syringe tubes were left in these holes to allow gas created through the dissolution process to safely escape. At each pH (3 and 7), one set of runs was performed with 380 x 6 mm borosilicate beads in the mill as abraders, and one set of runs was done without beads. The beads weighed an average of 0.2535 g, giving them a density of 2.24 g cm^3. A bedload of 380 beads was chosen as tests before the experimental runs displayed that this number struck a balance between the tools and cover effects. This gave a concentration of 1.21 beads per cm^2 of the disk. The shape of the flow, creating a circular flow around the centre of the disk, meant that the centre of the disk had a double layer of beads, whereas further out had either a single layer, or no layer.

All abrasion mill runs were performed for 35 hours. This run time was chosen after tests to place the runs that combined abrasive and chemical processes between 5 and 10 grams of mass loss, as suggested by the Turowski et al. (2023a) paper that aimed to standardize the procedure of working with an abrasion mill. The pH 7 runs were left for 35 hours with no interruptions. The pH 3 runs were performed through five 7-hour runs to allow for the mill solution to be topped-up with HCl every three and a half hours, as this was found to be the average time it took the solution to rise to pH 7. This kept the pH between 3 and 7 for the entirety of the 7 hour runs (mean 4.3, SD 1.5). This time interval was determined during previous testing through the creation of buffer curves, where the pH was measured at 15-minute intervals from pH3 until buffered with and without beads added. The disks were left covered in deionised water between each 7-hour run.

At the end of each run, the solutions were siphoned out using a hand-pump siphon into large 6L beakers. This solution was filtered with 0.22 µm nylon membrane filters, with a 50 mL sample of the filtered solution being retained for cation analysis, performed as with the cube experiments. The mill cylinder and disk were then rinsed with fresh deionised water, which was caught and filtered as well to ensure all detached material was caught for analysis. The disk was placed in a tray of deionised water, and then the saturated weight was measured. The difference in saturated weights was used to calculate overall mass loss rates.

4.3.2 Measuring the mass loss suspended in the solution

Before the experimental runs began, the 0.22 µm nylon membrane filters were dried in a beaker for 24 hours at 100°C. They were kept in a desiccator until use. After each time the mill was drained, the solution was filtered, and the used filters were redried and measured again. The original dry weight of the clean filter papers was subtracted to get the mass of suspended solids left in the solution after the runs.

5. Laboratory Cube Results

5.1 Cube mass loss with varying pH and temperature

Figures 10a, and b show the mass loss from each individual 22-hour experimental run (in percent weight loss and grams, respectively) plotted against the average solution temperature across the respective 22-hour period. These experiments were all run with cubes with an edge length of 4 cm. There is no significant relationship between the temperature of the run and the mass lost (Figures 10a, b, and c). Low R^2 values (<0.01) coupled with high p-values (>0.85) demonstrate that there is not a significant linear trend in which changes in mass loss can be explained by the solution temperature. T-tests show the same lack of a significant relationship, with two tail t-tests returning p-values markedly over the threshold of significant difference of $p<0.05$, meaning that the null hypothesis cannot be rejected, and the probability that the difference between groups occurred due to random chance is high (Table 8). The median mass losses and standard deviation, in grams, for the lowest, middle, and highest temperature bands, respectively, are 0.04±0.11 g, 0.05 ±0.11 g, and 0.04±0.10 g.

Table 8: Results from the t-tests performed between each set of mass losses associated with each temperature band

Pair of temperature band data sets	**Mass loss in percent weight loss**			**Mass loss in grams**		
	p-value	df	t-stat	p-value	df	t-stat
Low and mid	0.75	22	0.33	0.74	22	-0.33
Low and high	0.86	22	-0.18	0.96	22	-0.06
Mid and high	0.89	22	0.14	0.78	22	0.28

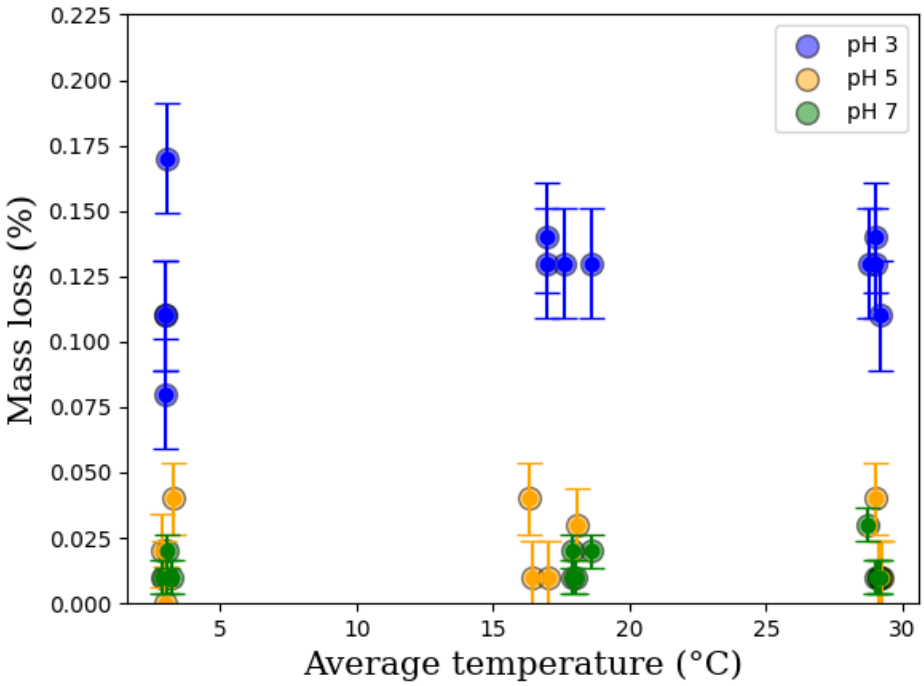

(a)

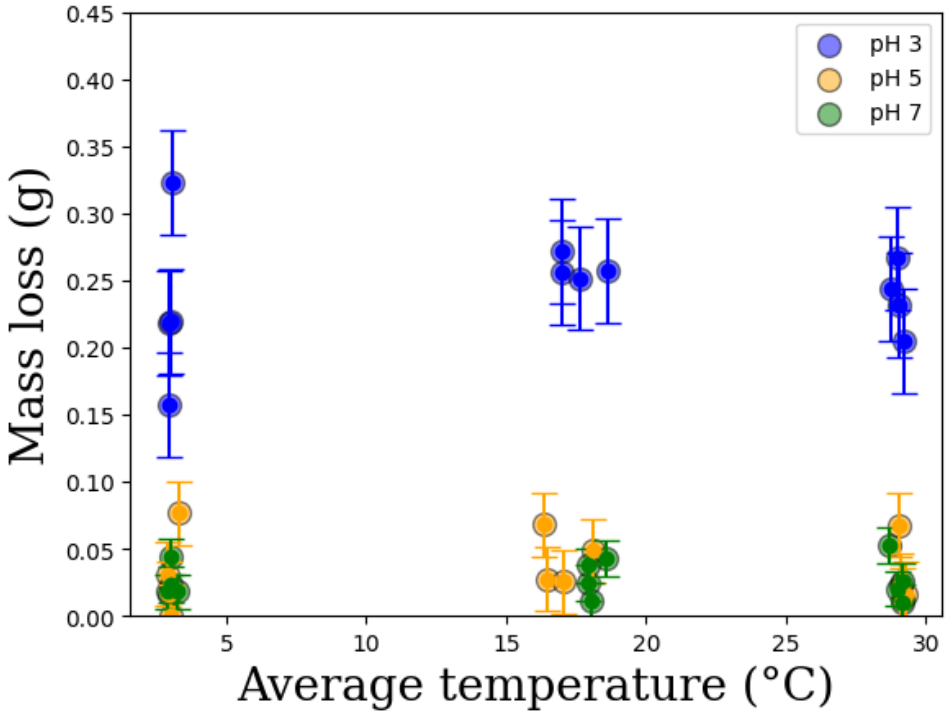

(b)

Figure 10: Plots showing the mass loss of the cubes in each 22-hour run in (a) percent weight lost and (b) grams lost depending on average temperature of the run. Each dot represents one 22-hour run. The error bars show one standard deviation above and below each data point.

The pH of the solution appears to have more of a relation to the mass loss than the temperature does. When plotted against pH, mass loss – in both grams lost and percent weight lost – shows a much clearer trend than with temperature (Figures 11a, b). There is a negative linear relationship between pH and mass loss reported in grams and percentage change, as shown by high R^2 values (0.72 for both). Low p-values (<0.01) for the linear regression show that this is a statistically significant trend. While the high R^2 and low p-values suggest a linear relationship between mass loss and pH, where higher mass loss occurs at a lower pH, they are better represented by a logarithmic relationship, which has a lower r-squared and p-value (R^2=0.80 and p-value <0.01 for both reporting methods, Figure 11). This would indicate that there is a threshold pH under which there is a rapid increase in dissolution rates, which makes sense as pH itself is a logarithmic function. This is supported by the t-tests performed that show a significant difference (p-values <0.05) between mass loss (in both reporting methods) caused by pH 3 and pH 5/pH 7, but no difference between mass loss caused by the pH 5 and pH 7 solutions (see Table 9). The median mass losses and standard deviation, in grams, for the pH 3, pH 5, and pH 7 runs, respectively, are 0.248±0.041 g, 0.027±0.025 g, and 0.024±0.014 g. The lower standard deviations for mass losses when related to pH also shows that pH is more determinate of mass losses, as the losses are less spread out, and therefore more related to each other.

Figure 11c shows that there are two outliers in mass loss in milligrams of the cubes submerged in pH 3 solution [defined as outside the range of Q1 (quarter 1 -- the 25th percentile) minus 1.5*IQR and Q3 (quarter 3 -- the 75th percentile) plus 1.5*IQR, where the IQR -- interquartile range—is the difference between Q3 and Q1]. These are both found in the pH 3 run dataset, one higher and one lower than the aforementioned range, both from the low temperature experimental runs. With and without them the pH 3 mass loss is statistically significantly higher than that of the runs at pH 5 or pH 7.

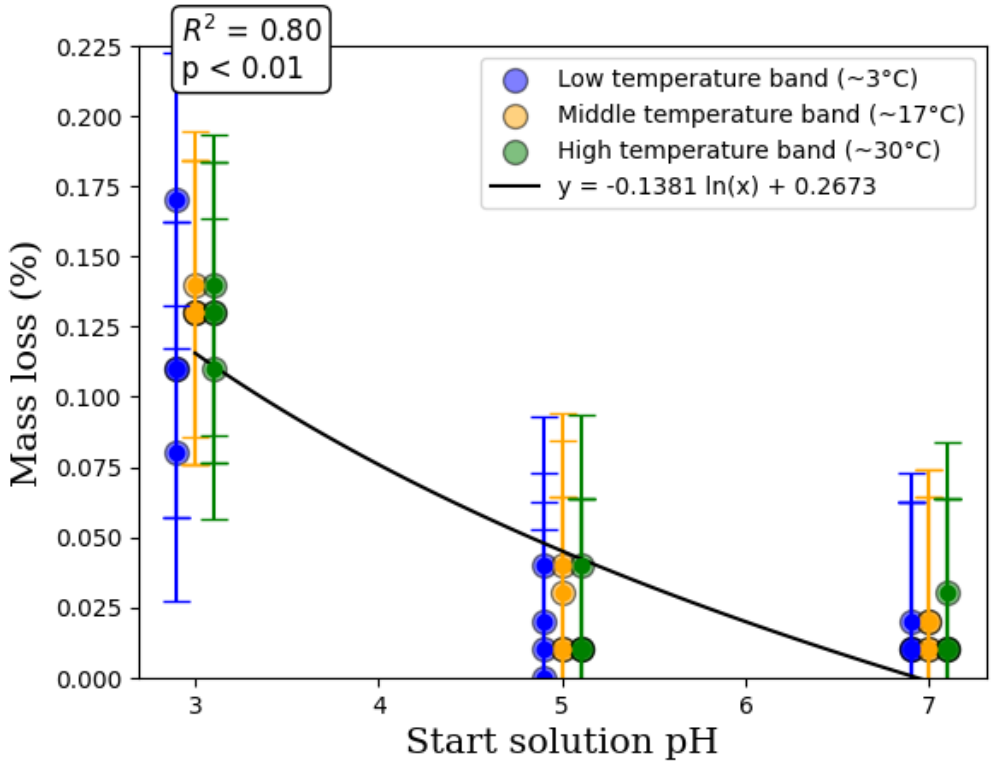
R^2 = 0.80
p < 0.01
Low temperature band (~3°C)
Middle temperature band (~17°C)
High temperature band (~30°C)
y = -0.1381 ln(x) + 0.2673
Mass loss (%)
Start solution pH

(a)

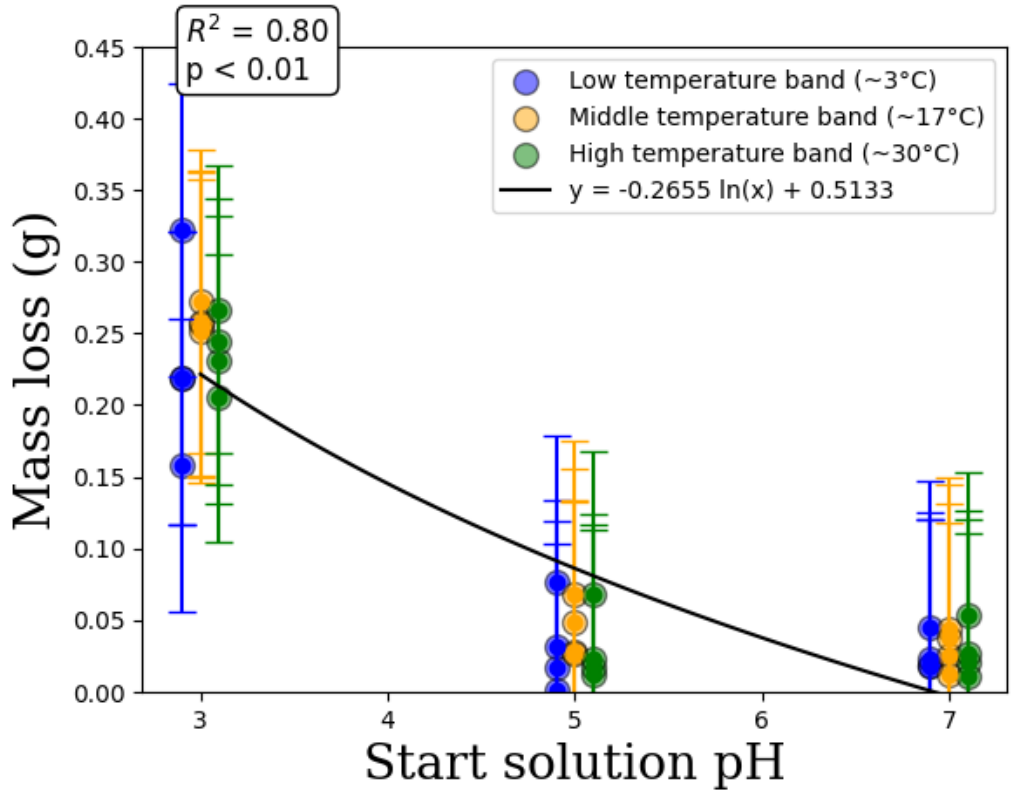
R^2 = 0.80
p < 0.01
Low temperature band (~3°C)
Middle temperature band (~17°C)
High temperature band (~30°C)
y = -0.2655 ln(x) + 0.5133
Mass loss (g)
Start solution pH

(b)

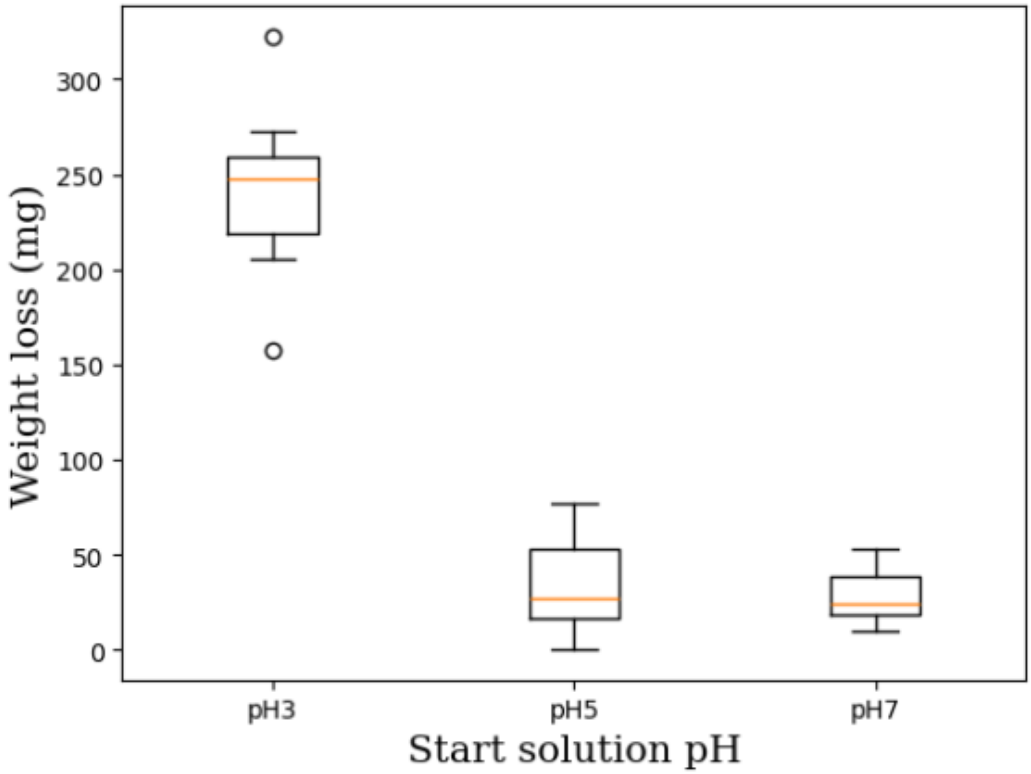

(c)

Figure 11: Plots showing the mass loss of the cubes in each 22-hour run for different starting solution pH in (a) percent weight lost and (b) grams lost, and (c) mg lost as a box and whisker plot. The orange line represents the median of the data, the edges of the box show the 25th and 75th percentile, with the whiskers extending out 1.5 times the IQR (difference between the 25th and 75th percentiles). Any data outside the whiskers are represented by circle and are considered outliers in the data set. In the scatter plots each dot represents one 22-hour run, and each temperature band has been slightly staggered to the sides of pH 3, 5, and 7 visually to make overlapping points easier to view. The scatter plots also have error bars, showing one standard deviation above and below each data point.

Table 9: Results from the t-tests performed between each set of mass losses associated with each solution pH

Pair of pH runs	**Pair of temperature band data sets**	**Mass loss in percent weight loss**			**Mass loss in grams**		
		p-value	df	t-stat	p-value	df	t-stat
3 and 5	Low and mid	<0.01	19	14.07	<0.01	18	15.09

3 and 7	Low and high	<0.01	13	16.87	<0.01	13	17.33
5 and 7	Mid and high	0.29	16	1.09	0.86	17	0.86

To test whether the mass loss rates achieved were indicative of longer-term dissolution rates, the set of four experimental runs for a 4 cm cube at room temperature in a solution starting at pH 3 were repeated an additional four times. For these runs, only the overall mass loss across the 88 hours was measured. For the original set of experimental runs, this mass loss over the 88 hours was 1.04 g, or 0.52%. In the four following weeks, the mass losses were 0.89 g (0.44%), 0.85 g (0.43%), 0.99 g (0.50%), and 0.93 g (0.47%). This shows no significant change in the mass loss across the 88-hours of dissolution as time continued, showing that the dissolution cube experiment results are likely indicative of longer term rates.

5.2 Solution cation trends

Analysis of dissolved calcium cation concentration in end solutions from the laboratory cube experiments corroborated the mass loss data graphed against temperature and pH. Similar to the relationships between mass loss and these controlling factors, temperature was not shown to be an explanatory factor for cation concentrations (p-value = 0.75), while starting solution pH was shown to have a statistically significant logarithmic relationship with cation concentrations the end of a 22-hour run (Figure 12c). Figure 12b suggested that there was a statistically significant relationship (p-value < 0.01) between cation levels and temperature of the run (when excluding the lowest pH runs), but that this relationship does not explain a high proportion of the variation in the cation concentration ($R^2 = 0.31$), showing limited predictive power of temperature over dissolved calcium levels, even at pH 5 and 7. The median cation concentrations and standard deviation, in mg L^{-1}, for the lowest, middle, and highest temperature bands, respectively, are 7.9±43.09 mg L^{-1}, 9.53±50.59 mg L^{-1}, and 12.38±46.37 mg L^{-1}. This high variability in cation concentrations in each temperature band shows that temperature does not appear to have strong correlation with calcium concentration. The median cation concentrations and standard deviation, in mg L^{-1}, for the pH 3, pH 5, and pH 7 runs, respectively, are 100.38±11.47 mg L^{-1}, 10.61±2.92 mg L^{-1}, and 7.58±1.54 mg L^{-1}. The lower standard deviations for cation concentrations related to pH also shows that pH is a better indicator of cation levels, as it means that the data is less spread within the pH groups, and therefore more related.

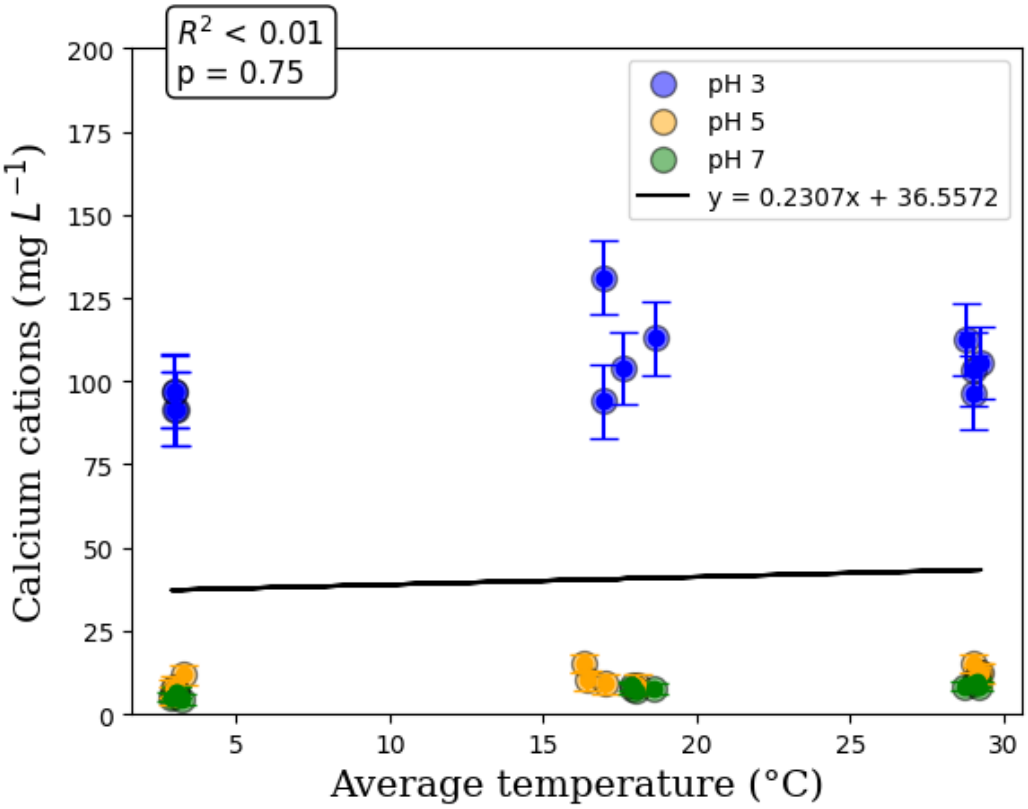
R^2 < 0.01
p = 0.75
pH 3
pH 5
pH 7
y = 0.2307x + 36.5572
Calcium cations (mg L^{-1})
Average temperature (°C)

(a)

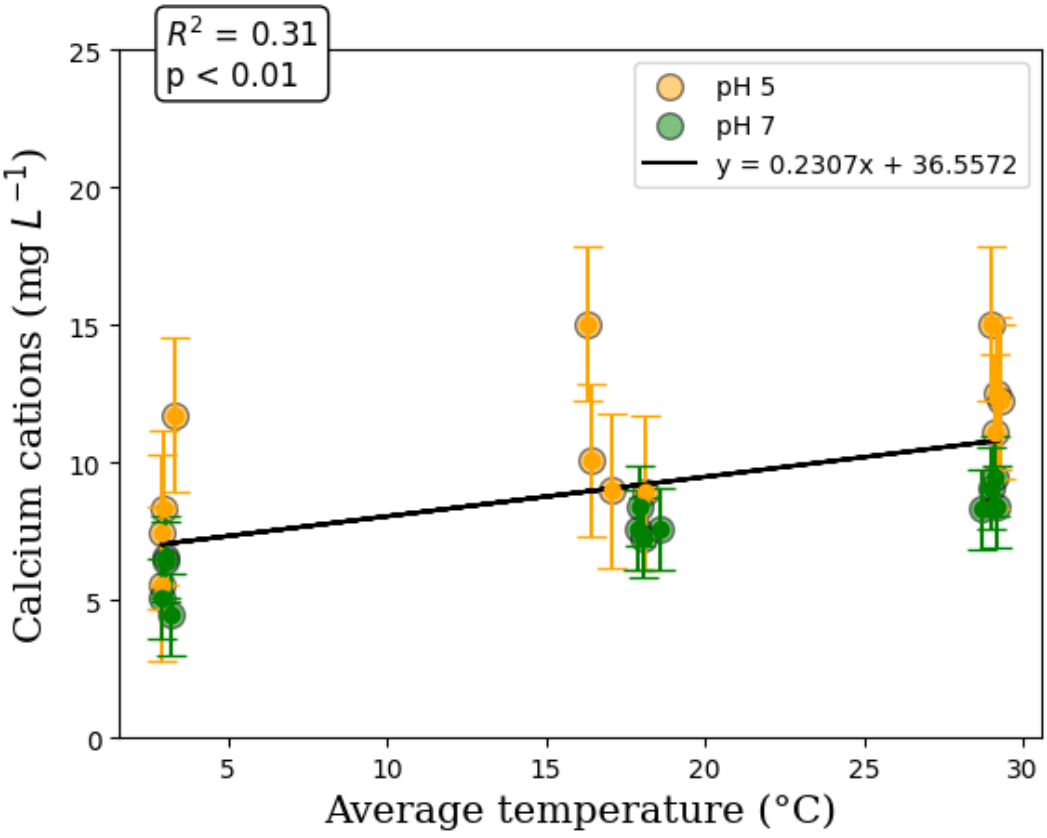
R^2 = 0.31
p < 0.01
pH 5
pH 7
y = 0.2307x + 36.5572
Calcium cations (mg L^{-1})
Average temperature (°C)

(b)

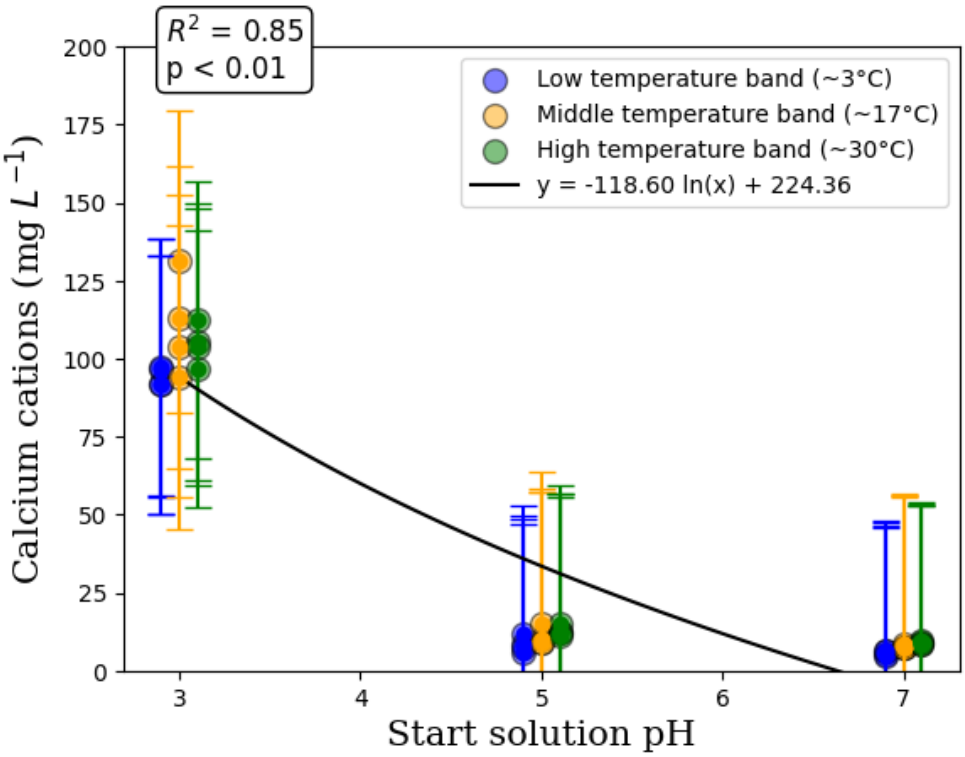

(c)

Figure 12: Plots showing the end solution cation levels of the cubes in each 22-hour run depending on (a) average temperature of the run, (b) depending on average temperature, but only at the two higher pHs, and (c) the starting pH of the run. Each dot represents one 22-hour run. The error bars show one standard deviation above and below each data point.

5.3 Buffering trends at different temperature points

There is a significant negative logarithmic relationship between the time it took the solution to buffer from pH 3 to pH 7 and the temperature of the solution, with a high proportion of variation in buffer time being explained by temperature (Figure 13, p-value <0.01, $R^2 = 0.96$). In addition, t-tests show that there is a statistically significant difference in buffer times at the low and high or low and mid temperature ranges, but no difference between buffer times at the mid (16.3° - 18,6°C) and high temperature (28.7°-29.3°C) ranges (see Table 10).

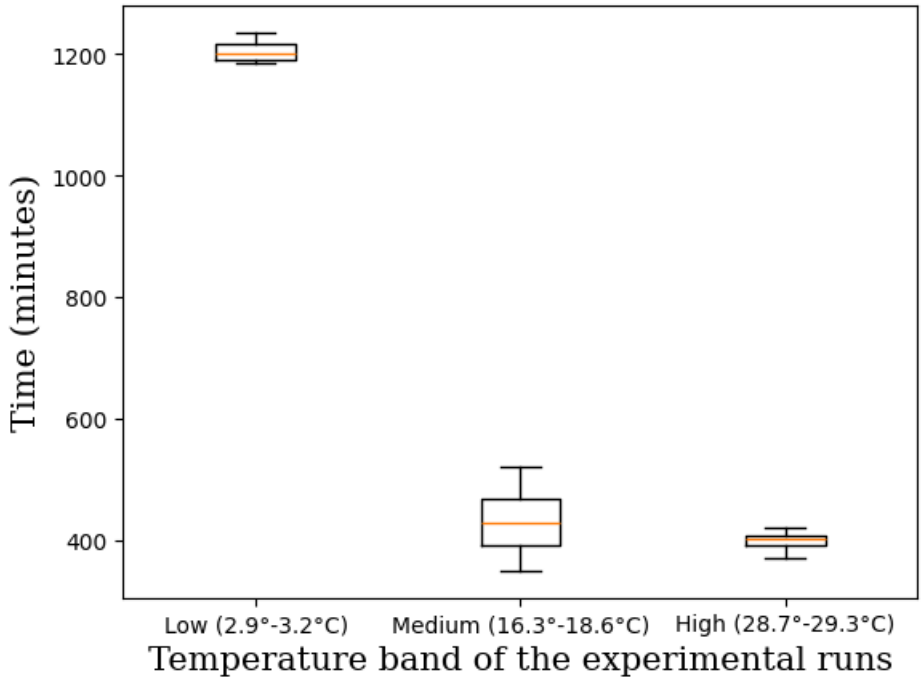

(a)

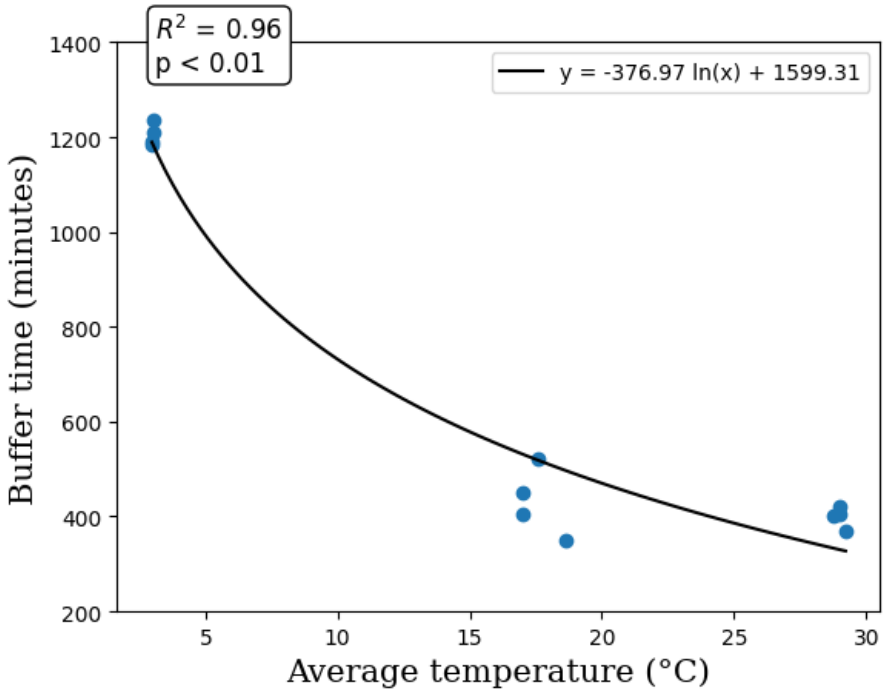

(b)

Figure 13: Plots showing the time it took for the solution to buffer from pH 3 to 7. 4a shows the buffer times in a box and whisker plot. The orange line represents the median of the data, the edges of the box show the 25th and 75th percentile, with the whiskers extending out 1.5 times the IQR (difference between the 25th and 75th percentiles). This data had no outliers, or points beyond the whisker range. Each dot represents one 22-hour run.

Table 10: Results from the t-tests performed between each set of buffer times (in minutes) associated with each temperature band

Pair of temperature band data sets	**Buffering times**		
	p-value	df	t-stat
Low and mid	<0.01	4	20.52
Low and high	<0.01	4	52.15
Mid and high	0.44	4	0.87

5.4 Surface area cube comparison

For each size of cube, 22-hour runs were performed on four replicates with the cubes submerged in circulating pH3 solution, at room temperature. There is a negative relation between mass loss and cube edge size (Figure 14a). To isolate the effects of cube surface area on reported mass loss results, mass loss was normalised as a percentage of total cube mass (Figure 14b) and for cube surface area (Figure 14c). This negative relationship was found regardless of whether mass is reported as grams lost, percent mass loss, or grams per cm^2 , however low R^2 values (<0.55) show a weak overall fit. The variation in mass loss as reported by percent weight loss and g cm^{-2} showed that cube edge length was a statistically significant indicator for mass loss, with p-values below 0.05 (Figures 14a and 14c), whereas the variation in mass loss in grams was not significantly explained by the change in cube edge length (Figure 14b, p-value = 0.49).

Table 11: Key attributes of the limestone cubes

Average cube edge length (cm)	**Surface area (cm^2)**	**Volume (cm^3)**	**Surface area/volume ratio**	**Ca composition**
3	54	27	2.0	448,170 - 448,544 ppm ±2193-3206
4	96	64	1.5	
5	150	125	1.2	

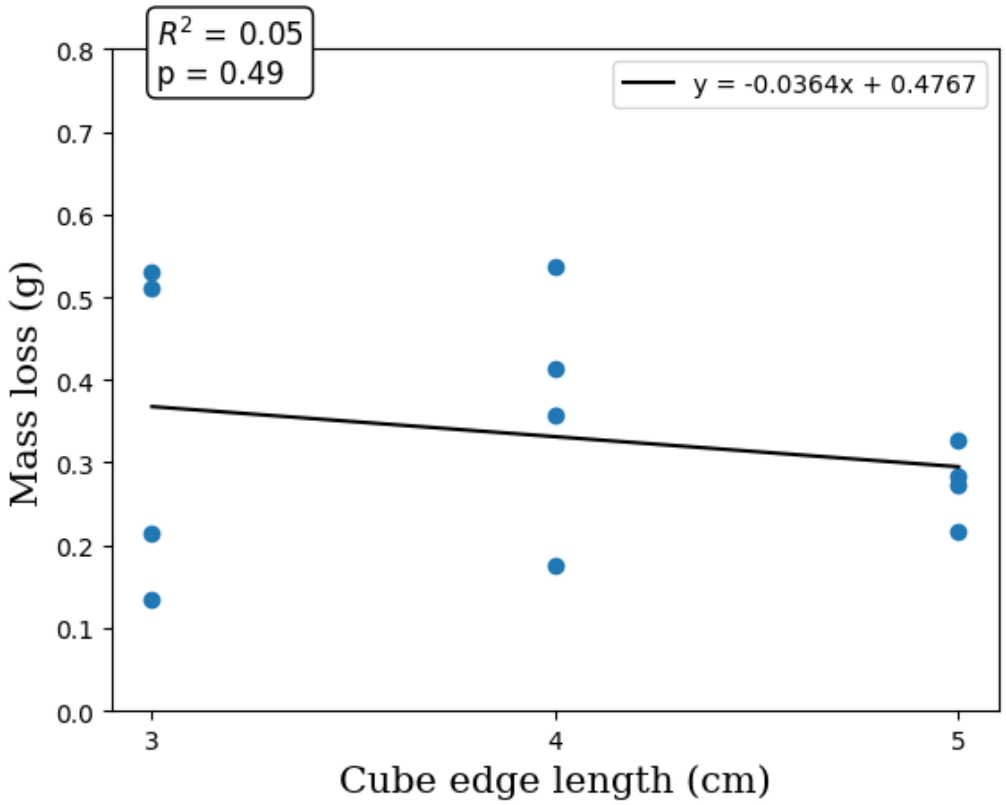
R^2 = 0.05
p = 0.49
y = -0.0364x + 0.4767
Mass loss (g)
Cube edge length (cm)
0.0
0.1
0.2
0.3
0.4
0.5
0.6
0.7
0.8
3
4
5

(a)

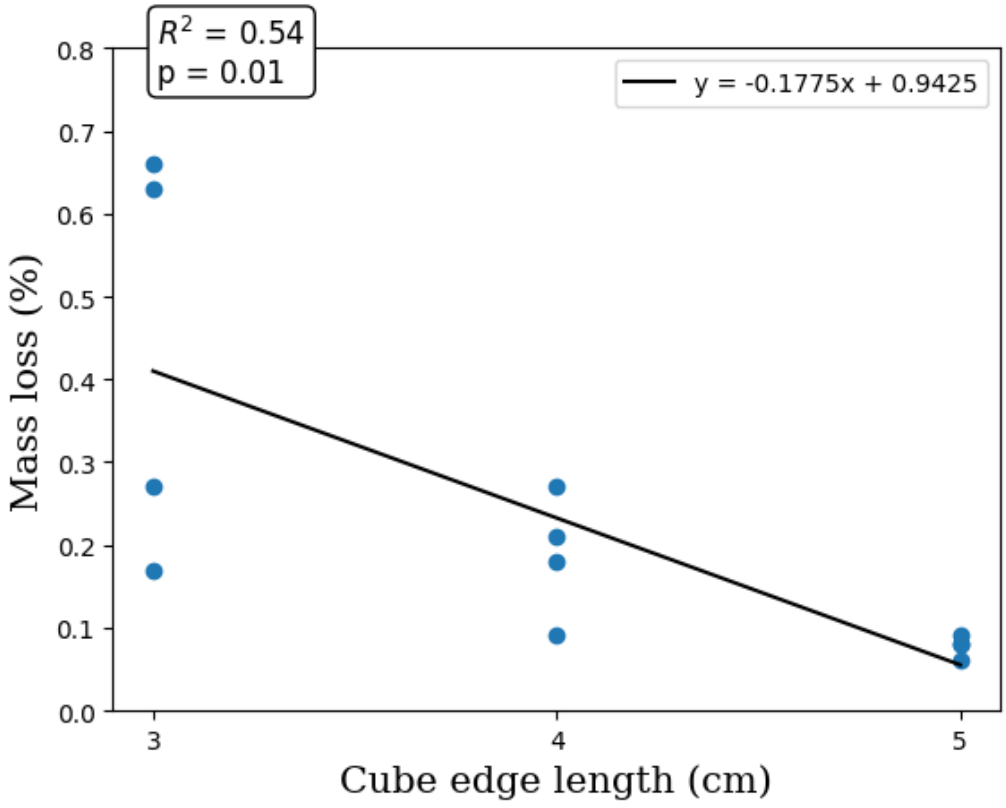
R^2 = 0.54
p = 0.01
y = -0.1775x + 0.9425
Mass loss (%)
Cube edge length (cm)
0.0
0.1
0.2
0.3
0.4
0.5
0.6
0.7
0.8
3
4
5

(b)

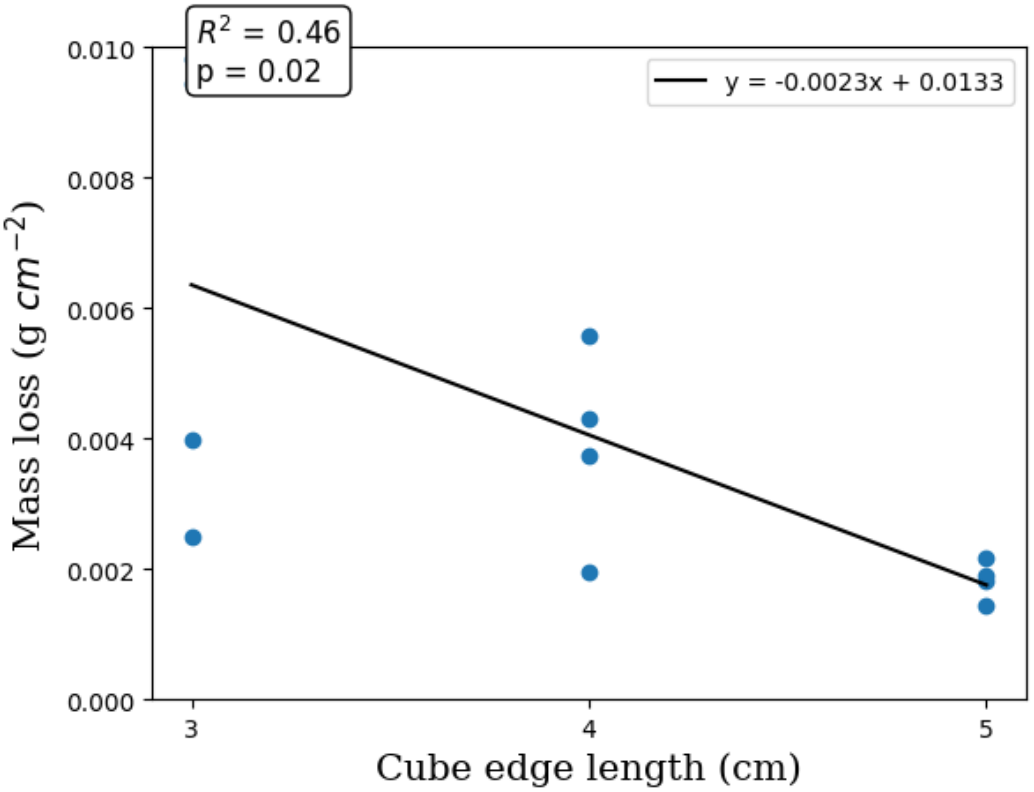

(c)

Figure 14: Mass loss for different cube sizes in (a) grams, (b) percent change, and (c)g cm^{-2}

6. Abrasion Mill Results

6.1 Mass loss across different pH and sediment supply conditions

The greatest mass loss in the abrasion mill was observed under the lowest pH conditions, where abrasive tools were also present (Table 12 and Figure 15). The total mass loss (6.47 g) was just lower than the combined mass losses from the lowest pH run with no abrasive tools (3.64 g) and neutral pH run with abrasive tools (3.05 g). The control run performed with pH 7 deionised water and no beads only produced 0.2 g of total mass loss, showing the minimal effect of chemical and physical processes in a neutral environment with no abraders. In every run the dissolved load was higher than the suspended load, with the pH 7 run with beads having the highest proportion of suspended load (30%). This domination of dissolved load at neutral pH is unexpected, as abrasion was expected to account for more of the mass loss. The lowest suspended load proportion was for the pH 3 run with no beads, where only 2% of the mass loss was through suspended load.

At pH3 and pH 7, adding beads into the mill increased the overall mass loss, and increased the suspended load by tenfold, but also resulted in increased dissolved load, from 0.15 to 2.15 g for pH 7 and 3.55 to an average of 5.58 g for pH 3. At either bedload concentration, however, changing the start pH from 7 to 3

increased the dissolved load by 30 times with no beads and 3 times with beads, but the suspended load did not have a similar increase (~2 times with no beads, and no discernable increase with beads). Both the suspended and dissolved load were susceptible to changes in abrasive load, but only dissolved load showed noticeable increases with changes in pH.

The two 35 hour runs performed with pH3 solution with the abrasive bedload produced similar proportions of suspended versus dissolved load, with the second experimental run having 37% higher dissolved load (6.84 g vs 4.33 g) and 3% higher suspended load (0.90 g vs 0.87 g). X-Ray Fluorescence (XRF) analysis performed on the two disks used for these runs showed that the second disk, with the higher dissolved mass loss, had a 15% higher calcium content (199,500±1,900 vs 169,800±1,800 ppm). This slight imbalance in the calcium content of the two disks is likely what contributed to this difference in total and dissolved mass loss in the two pH 3 with beads mill runs. This is corroborated by the calcium content of the end solution from the second disk being on average 25% higher than that for the first.

Table 12: Total mass loss, mass loss rate, suspended loss, and dissolved loss from the abrasion mill runs with 1[ce]:1[sa]:1[sh] disks, starting average calcium content of 260,891 ± 2,204ppm

Combination	**Overall mass loss (g)**	**Loss rate (g hr $^{-1}$)**	**Suspended loss (% of total mass loss)**	**Dissolved loss (% of total mass loss)**	**Average calcium content in solution after 7 hours (mg L^{-1})**
pH 3, with beads (run 1)	5.20	0.15	0.87 g (17%)	4.33 g (83%)	90.55
pH 3, with beads (run 2)	7.74	0.22	0.90 g (12%)	6.84 g (88%)	113.26
pH 3, with beads (average of the 2)	6.47	0.18	0.89 g (14%)	5.58 g (86%)	101.91
pH 3, with no beads	3.64	0.10	0.09 g (2%)	3.55 g (98%)	66.04
pH 7, with beads	3.05	0.09	0.90 g (30%)	2.15 g (70%)	n/a
pH 7, with no beads	0.20	0.01	0.04 g (22%)	0.15 g (78%)	n/a

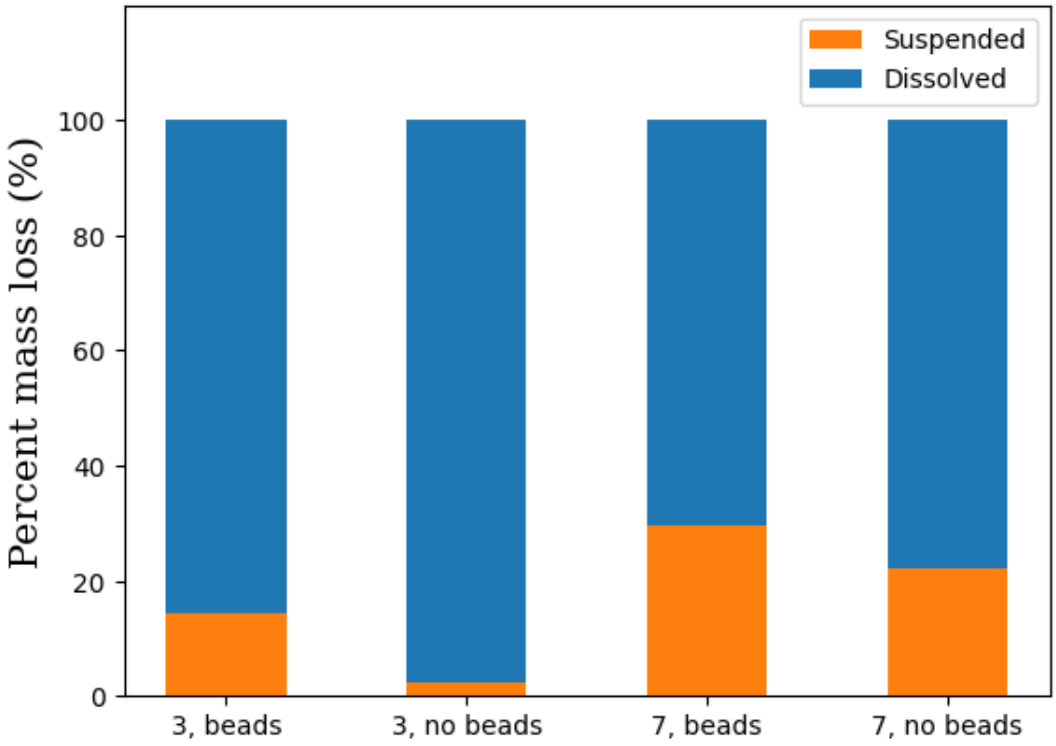

(a)

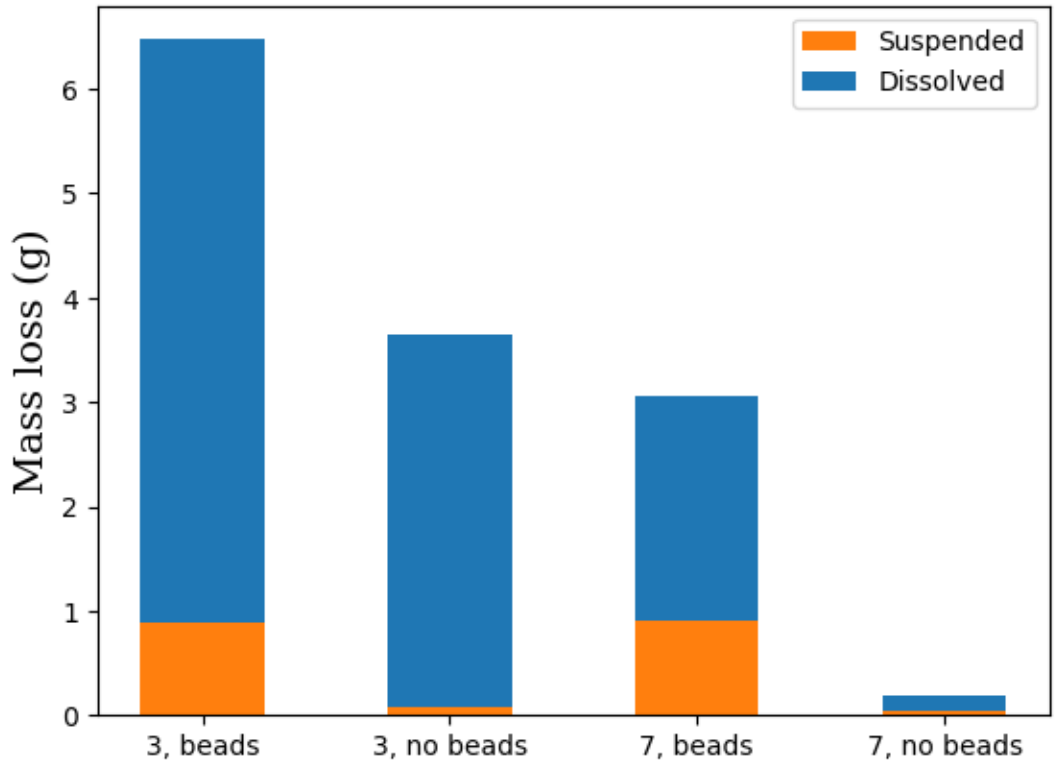

(b)

Figure 15: Bar charts showing the proportion of the total mass loss from each 35-hour run that was produced through suspended and dissolved load in (a) percentage and (b) grams

As disk mass was not measured at the end of each 7 hours of runtime, the cation levels tell us how even the dissolution was across the 5 days that the experiments were run. Figure 16 shows that there is no significant linear relationship between the day of the experiment and the cation levels, with a low R^2 (0.07) and high p-value (>0.05).

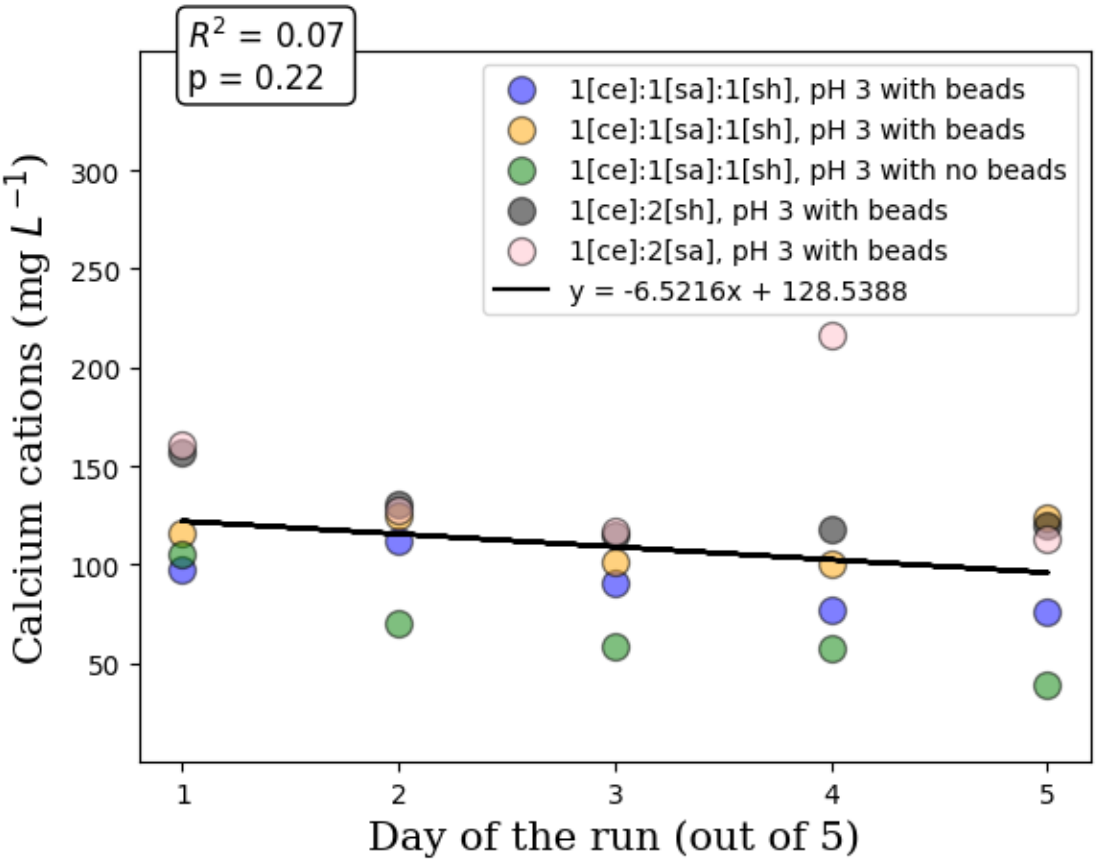

Figure 16: Plot showing the solution cation levels of abrasion mill solution at the end of each 7-hour day.

6.2 Mass loss across different carbonate content

The abrasion mill mass loss results across the three experimental runs ran with different rock compositions, all at pH3 with abrasive load, showed different mass losses and proportions of suspended and dissolved load (Table 13, Figure 17). The 1[ce]:2[sa] disk had the highest overall mass loss of 14.29 g, and the highest suspended load proportion, at 42%. The 1[ce]:2[sh] disk had the next highest overall mass loss, with 9.08 g total loss, and had the highest proportion of dissolved load at 94%. This aligns with their calcium content, as the 1[ce]:2[sa] disk had only 73% of the calcium content that the 1[ce]:2[sh] disk had, meaning that the sand-rich disk was less susceptible to dissolution. The [ce]-1[sa]-1[sh] disk has an

intermediate total mass loss value, and intermediate proportions of suspended and dissolved mass losses compared to the other disks. values of total, suspended, and dissolved mass losses. As the 1[ce]:1[sa]:1[sh] composition disk has an intermediate calcium content, it fits that the proportion of dissolved to suspended load is between the two others. The average dissolved calcium content at the end of each 7-hour portion of the 35-hour runs was highest for the 1[ce]:2[sa] disk, then the 1[ce]:2[sh] disk, then the 1[ce]:1[sa]:1[sh], even though the 1[ce]:2[sh] disk has the largest mass loss through dissolution (Table 13).

Table 13: Total mass loss, mass loss rate, suspended loss, and dissolved loss from the abrasion mill runs with 1[ce]:1[sa]:1[sh], 1[ce]:2[sa], and 1[ce]:2[sh] disks

Disk Composition	**Calcium content (ppm)**	**Overall mass loss (g)**	**Loss rate (g hr^{-1})**	**Suspended loss (% of total mass loss)**	**Dissolved loss (% of total mass loss)**	**Average calcium content in solution after 7 hours (mg L^{-1})**
1-1-1 (average of two runs)	260,891 ± 2,204	6.47	0.18	0.89 g (14%)	5.58 g (86%)	101.91
1-2 (cement:sand)	251,177 ± 2,087	14.29	0.40	6.01 g (42%)	8.28 g (58%)	146.91
1-2 (cement:shell)	345,733 ± 2,719	9.08	0.26	0.57 g (6%)	8.50 g (94%)	128.10

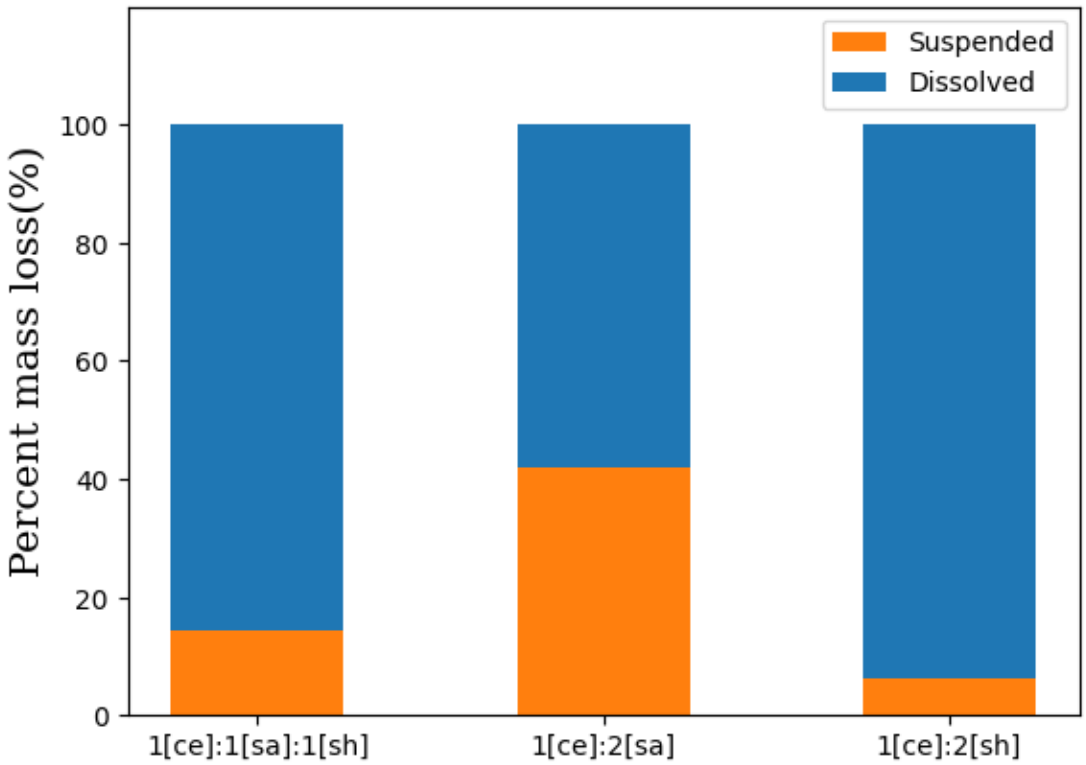

(a)

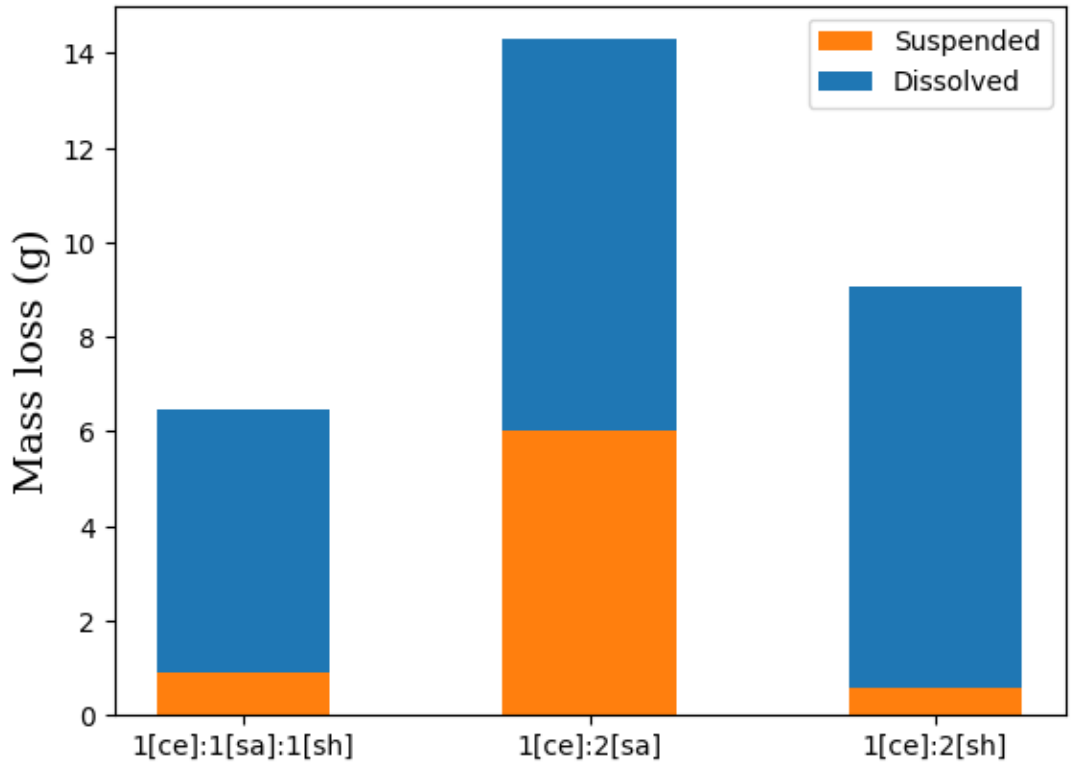

(b)

Figure 17: Bar charts showing the proportion of the total mass loss from each 35-hour run that was produced through suspended and dissolved load in (a) percentage and (b) grams

7. Field Results

7.1 Mass loss

Table 14 shows the mass loss of limestone and sandstone cubes within Trout Beck in the North Pennines. The dry weights after inundation were taken after 2 weeks in the 40°C oven and then again after another week, so that they were confidently dry as there was less than a 0.02% weight change between the two measurements. For the limestone cubes there was an average of 1.08, 1.56, and 0.18 g lost per cube in the pool, on the bench, and in the atmosphere, respectively. This provides average mass loss rates of 3.29, 4.75, and 0.55 g yr^{-1} assuming these rates are sustained across the full year. The sandstone cubes lost less mass than their limestone counterparts, at 0.55 g in the pool, 0.25 g on the bench, and 0.12 g on the bank. Figures 18a, b, and c show the spread of mass loss in grams, percent change, and grams per cm^2 for the limestone cubes in each position. This, similarly to the average mass losses, shows that the cubes on the bank in the atmosphere lost less mass than those in the pool or bench. However, these differences were not statistically significant, with the difference between percent weight loss on the bench and on the bank being the only relationship found to be significant ($p<0.05$, Table 15).

Table 14: Total mass loss (in three reporting methods) and mass loss rate for cubes in the river channel, according to position, size, and lithology

Location	Rock type	Cube edge size (cm)	Mass loss (g)	Weight loss (%)	Mass loss (g cm^{-2})	Mass loss rate (g yr^{-1})
Pool	Limestone	8	1.34	0.09	0.00028	4.08
	Limestone	5	1.7	0.49	0.011	5.17
	Limestone	3	0.2	0.28	0.0037	0.61
	Sandstone	7	0.55	0.07	0.0019	1.67
Bench	Limestone	8	3.55	0.27	0.0092	10.81
	Limestone	6	0.82	0.13	0.0038	2.50
	Limestone	4	0.32	0.20	0.0033	0.97
	Sandstone	6	0.25	0.05	0.0012	0.76
Atmosphere	Limestone	9	0.4	0.02	0.00082	1.22
/Bank	Limestone	7	0.2	0.02	0.00068	0.61
	Limestone	5	0.09	0.02	0.00060	0.27
	Limestone	3	0.02	0.03	0.00037	0.06
	Sandstone	5	0.12	0.04	0.00080	0.37

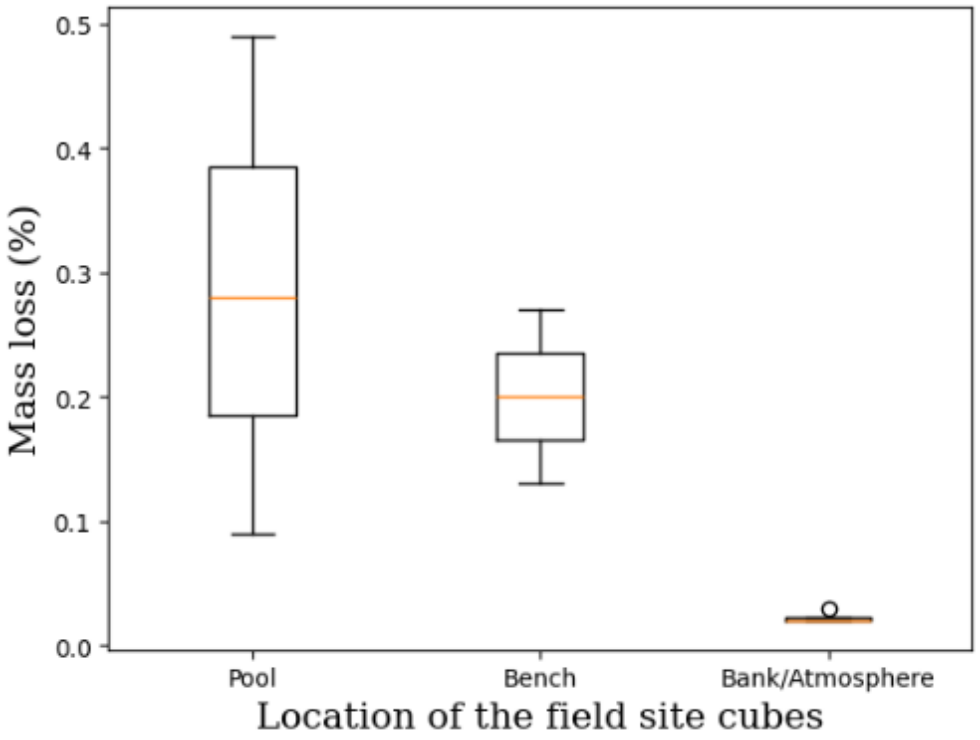
0.5
0.4
0.3
0.2
0.1
0.0
Mass loss (%)
Pool
Bench
Bank/Atmosphere
Location of the field site cubes

(a)

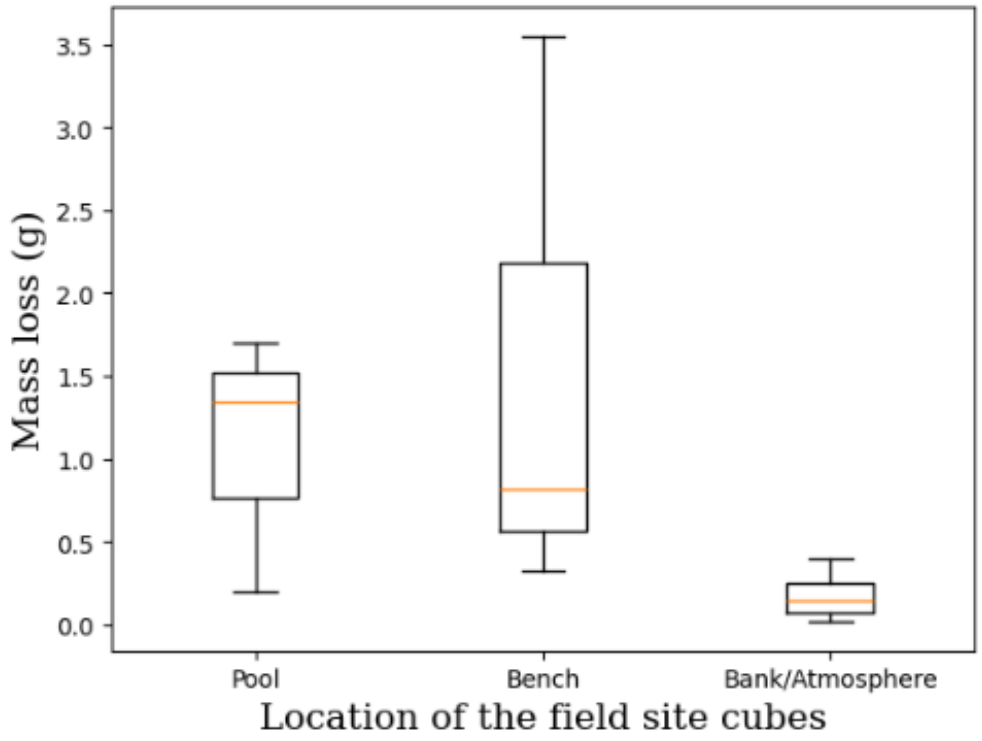
3.5
3.0
2.5
2.0
1.5
1.0
0.5
0.0
Mass loss (g)
Pool
Bench
Bank/Atmosphere
Location of the field site cubes

(b)

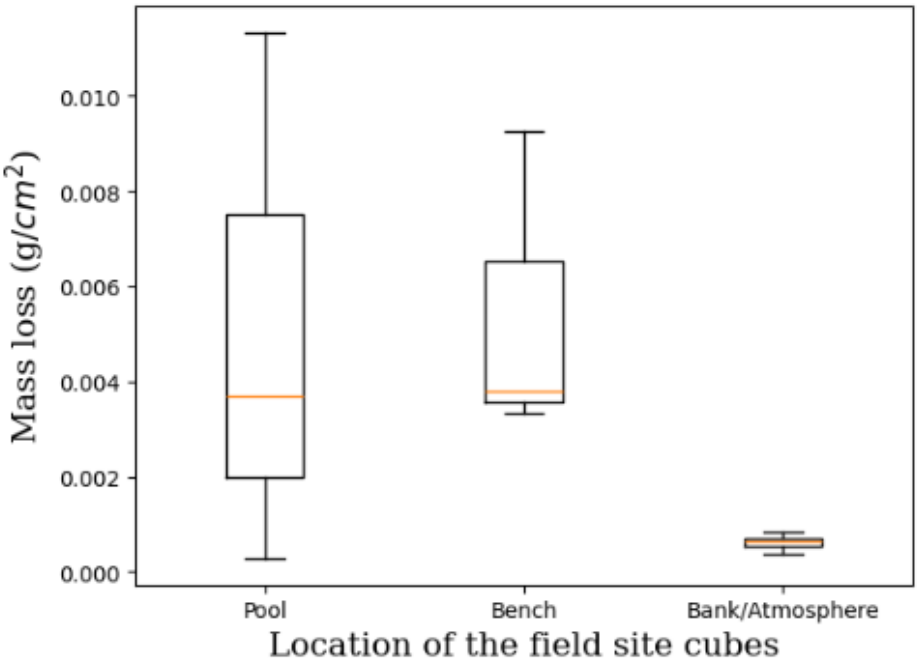

(c)

Figure 18: Plots showing the mass loss of cubes suspended in different sections of Trout Beck for 120 days, with mass loss reported in (a) percent change, (b) grams lost, and (c) grams per cm^2. The orange line in these box and whisker plots represent the median of the data, the edges of the box show the 25th and 75th percentile, with the whiskers extending out 1.5 times the IQR (difference between the 25th and 75th percentiles). The circle in 7b shows an outlier in the data, where it is beyond the whisker range.

Table 15: Results from the t-tests performed between each set of mass loss data of limestone cubes within each position

Pair of position data sets	Percent change			Grams			Grams cm^{-2}		
	p-value	df	t-stat	p-value	df	t-stat	p-value	df	t-stat
Pool and bench	0.53	3	-0.44	0.69	2	0.72	0.93	3	-0.09
Pool and bank	0.15	2	1.96	0.18	2	2.26	0.30	2	1.37
Bench and bank	0.05	2	1.38	0.30	2	4.44	0.13	2	2.55

8. Discussion

Both sets of laboratory dissolution experiments showed clear, consistent indications of which environmental and lithological factors (i.e. calcium content, grain size distribution of mineral components, and tensile strength) are important in the erosion of bedrock river channels. The submersion of limestone and sandstone cubes in the field site also identified that rates of bedrock erosion occur differentially across different heights in a river channel, that correlate to different immersion frequencies and intervals. The following chapter considers how findings from the laboratory and field work combine to create a more complete view of how different controls on chemical and physical erosive processes in bedrock rivers occur. This is achieved by testing the original hypotheses discussed in Section 3.

8.1 What environmental factors (pH, temperature, immersion time) control the dissolution rates of limestone in laboratory cube experiments and river channel field tests?

The combination of laboratory and field results, over similar temperature and pH ranges, creates better understanding of what controls the erosion of limestone in fluvial systems. Changing the temperature and starting solution pH of the limestone cube dissolution experiments indicated that pH is a significant control on chemical weathering rates, while at the temperature range tested (3°-30°C), temperature is not a significant control. In past studies, increasing temperature (0° to 1000°C and 25° to 80°) has been linked to higher dissolution rates (Oelkers and Helgeson, 1988; Alkattan et al., 1998), consistent with Arrhenius kinetics (Equation 4). This temperature dependence reflects the requirement that activation energy barriers at the calcite-water interface must be overcome to facilitate proton (H+) or carbonic acid attack on carbonate groups and ultimately release calcium cations and carbonate species into solution (Oelkers and Helgeson, 1988; Kohitlhetse et al., 2021). However, the cube experiments showed no significant difference between mass loss at ~3°C, 17°C, and 30°C. Past study has shown that at near neutral pHs (8.4), calcite dissolution increases between 5°C and 25°C, with a direct correlation found between release of calcium and temperature (Yadav et al., 2008). Continued study, looking at silicon dissolution across the same temperature range, but at pHs of 2.2, 4.0, and 8.4 found that the increase in dissolution rate across the temperature range decreased as the pH lowered (Yadav et al., 2008). Therefore, at lower pHs, like the ones used in most of the laboratory cube experiments performed, the reaction pathways have low activation energy, and dissolution is controlled by H+ concentrations, rather than temperature within the 30°C range tested here.

$$k = Ae^{-E_a/RT}$$

Equation 4: Arrhenius equation relating the activation energy (E_a) to the rate constant (k) and temperature (T) in Kelvin, where A is the pre-exponential factor and R is the gas constant

This previously theorized and tested relationship between temperature and pH in dissolution dynamics, where pH has a higher control over dissolution rates than temperature, was shown in the cube dissolution experiments, where pH was shown to be a statistically significant predictor of mass loss when fitted to a logarithmic or linear function. A statistical difference was found between mass losses of cubes suspended in pH 3 and pH 5/pH 7 solutions, whereas no significant difference was found between mass loss with a starting solution pH of 5 versus 7. The lack of statistical difference between mass losses caused by pH 5 and pH 7 solutions points to a threshold response, in which mass loss significantly increases when pH drops below a certain value. This is likely due to activation energy dynamics, in which at pH 3 the activation energy required to start the chemical reaction of dissolution is very low, as there is a high supply of H+ protons to attack the carbonate rock. However, at pH 5 and 7 there are less protons available than at pH 3, so a high activation energy is required to start the dissolution process. As shown in Table 16, this study's dissolution rates from the cubes were, from pH 3, on average 10-52 times less than those found by Alkattan et al. (1998). Alkattan et al. (1998)'s experiments included a flow through component that kept the pH at 1 the entire run, so this difference is likely due to that lower pH. Dong et al.'s 2024 study, using a flow through mechanism at pH 4.2, produced cation outputs significantly lower than this study's at any of the pH and temperature combinations tested.

Table 16: Cube experiment dissolution rates in this study, and previous laboratory dissolution experiments, all performed on limestone

Source	pH range	Solution temperatures	What was measured?	Reported dissolution rates	Reported end cation concentration
This study	**3, 5, 7**	**3°C, 17°C, 30°C**	**Mass loss**	**0.0283 (3°C, pH 7) – 0.2830 (17°C, pH 3) g d^{-1}**	
			Calcium ion output		**6.13 (3°C, pH 7) – 120.58 (17°C, pH 3) mg L^{-1} d^{-1}**
Alkattan et al. (1998)	1	25°C	Mass loss	2.829-13.9596 g d^{-1}	
Hattanji et al. (2014)	Neutral pH, different flow rates	20°C	Ca ion output		0.037±0.002 through 0.124±0.007 mg cm^{-2} d^{-1}
Dong et al. (2024)	4.2	Room temperature	Ca^{2+} ion changes		0.0858 to 3.9602mg L^{-1} d^{-1}

The results of the cube experiments run at ~3°C corroborated the evidence that has emerged in the last century about the potential impacts of chemical weathering in cold or glacial environments. Many glacial locations have shown clear weathering rinds on valley walls, as well as other marks of chemical weathering such as cation analysis on outflowing waters (Hoch et al., 1999; Hodson et al., 2010; Dabski et al., 2019; Gaillardet et al., 2019). There was no difference found in the mass loss (in grams or percentage change) between the cubes suspended in 3°C solution versus either 17° or 30°C, showing that chemical dissolution occurs at near freezing temperatures. However, the difference in buffer times for the cold cube runs shows that rates may not be the same. While overall mass loss, and therefore average dissolution rate, were found to not be statistically different at the low, medium, and high temperature bands, it took the low temperature solution more time to buffer from pH 3 to pH 7 than the other two temperatures. It took roughly triple the time for the low temperature solution to buffer, with an average time of 20 hours and 5 minutes versus 7 hours 11 minutes and 6 hours 38 minutes for middle and high temperature respectively. As acid was only added at the start of each 22-hour experimental run, the mass loss rates are averaged out across the 22-hours in which there is a faster dissolution rate at the start, moving on to lower rates as solution gets closer to saturated from the calcium. Due to the longer buffer times at 3°C, where the solution takes over 20 hours on average to reach pH 7, it can be assumed that the actual point dissolution rates would spread less away from the averaged mass loss rate reported from these runs than at the higher temperatures. This means that if the experiments had been performed with a flow-through element, in which the pH was topped up continuously throughout the run not allowing the solution to buffer, the higher temperature runs would likely lead to more mass loss, and higher resultant rates, than at the lower temperature. When the mass loss rate is calculated as overall mass loss divided by buffering times, the losses are 0.0114 g hr^{-1}, 0.0361 g hr^{-1} and 0.0357 g hr^{-1} for 3°C, 17°C, and 30°C respectively, showing that temperature may have an effect on dissolution rates in a system where there is a more constant supply of acidic solution. However, the 3°C run mass loss does show that dissolution occurs at near zero temperatures.

In the field experiments, the average mass loss from the cubes in the pool and bench locations was higher than that on the bank in the atmosphere. The pool cubes were immersed for the duration of the 120 days, due to their positioning upstream of a sill that maintained water levels in the pool ever during low-discharge conditions. Based on averaged daily gauged flow data from Trout Beck, scaled as described in the methodology section, over the 120-day period the bench cubes were immersed for 4 days (96 hours), and the bank cubes were never in the flow. The cubes attached to the bench lost an average of 1.56 g per cube, whereas the pool set of cubes lost an average of 1.08 g each. Given the pool cubes were inundated

for more time, they were expected to have a larger rate of mass loss than those on the bench, as longer submersion means more time for chemical dissolution reactions to occur.

The higher discharge flows that inundated the bench cubes may have had a high dissolution potential the than the slower ones that consistently covered the pool cubes. The bench cubes were 20 cm from the river floor and were only inundated when the river had a discharge of 0.76 $m^3 s^{-1}$. The cubes in the pool were only 5 cm above the bed, meaning that a flow of 0.04 $m^3 s^{-1}$ would submerge them. The flows that immersed the bench cubes were faster with higher discharge, meaning that the diffusion boundary layer thinned, preventing the reaction of dissolved CO2 with H+ molecules closer to the surface of the flow, and allowing the carbonic acid and loose H+ protons to interact with the surface of the limestone bedrock (Equations 2 and 3), where the cubes were positioned (Liu and Dreybrod, 1997). This means that a larger proportion of the dissolution happening in the pool cubes would also occur during these higher flows, where the chemical ions are able to travel more freely across the diffusion boundary. The detached calcium cations in solution occurring due to dissolution of limestone surfaces are more prone to cross the diffusion boundary layer and react with dissolved CO_2 when it is thinner (Liu and Dreybrod, 1997), limiting further dissolution, but high velocity flows that create the thinner boundary can also flush these cations away. High velocity flows have also been correlated with increased CO_2 take up from terrestrial sources, as well as drawdown from the atmosphere, through creating turbulence at the air-water interface (Leng et al., 2020), further showing that the high velocity/discharge floods have a higher dissolution potential.

As the bench cubes lost more mass on average than the pool cubes, wetting-drying cycles likely had a large effect on the mass loss that happened for the bench set. Wetting-drying cycles have been shown to contribute to physical breakdown, as the cycles of swelling and contracting of the rock pores leads to rock weakening, leaving it more prone to other erosional forces, as well as breaking off material itself (Gregory, 2010; Bared et al., 2020; Gu et al., 2021). The four days that the bench cubes were inundated were between 4 and 85 days apart, giving them time to dry between wetting cycles, meaning that this method of breakdown was likely the dominant physical weathering process occurring, as the cubes were set in a mesh cage that would have largely protected them from abrasion. The increased mass loss for the bench cubes could also have occurred due to acidic run off from the peat reacting with the cubes (Banas and Gos, 2004). Any runoff interacting with the pool cubes would undergo high levels of dilution in the stream water, leading to a weaker acid, and therefore lower level of dissolution, as seen in the laboratory cube experiment results.

As seen in Table 17 below, the mass loss rates are roughly comparable to past research performed using submerged, and non-submerged, limestone tablets in the field. Cahoon et al. (1993) completed a similar cube mass loss field experiment, comparing mass loss rates of limestone tablets suspended at the mouth of a creek entering lake Waccamaw, USA, and those by a limestone wall in the lake across 108 days, fully submerged for the duration of the experiments in both locations. The average mass loss rates on the Trout Beck bench and in the pool are lower than rates reported in Cahoon et al. (1993) for the creek mouth, yet higher than those for inside the lake, in g yr^{-1}, but lower than all positions in percent loss (Table 15). The stream pH was reported as approximately 6.4, and the lake location had an average pH of 7.05 (Cahoon et al., 1993). Trout Beck's average of 6.7 sets it between the two positions within Lake Waccamaw, which correlates with the intermediate mass loss rates. Apart from the Cahoon et al. (1993) experiments, the cubes in Trout Beck (in all positions) lost a greater percentage of their mass than other listed tablet loss experiments in other fluvial and precipitation-based experiments (Table 17).

Table 17: Mass loss rates from natural tablet and cube dissolution experiments in fluvial systems

Source	Rock type	Temperature of the field site	Placement	What was measured?	Measurements
This study	**Limestone**	**-0.9° - 24.7°C**	**5 cm, 20 cm, and 5 m above riverbed**	**Averaged mass loss per cube in each location**	**In the pool: 3.29 g yr^{-1} (0.994 wt% yr^{-1})** **On the bench: 4.76 g yr^{-1} (0.9933 wt% yr^{-1})** **On the bank: 0.54 g yr^{-1} (0.9994 wt% yr^{-1})**
Hattanji et al. (2014)	Limestones	-0.9-22.9°C	3 streams (two non-limestone sources, 1 karst source)	Mass loss	<u>In non-limestone streams:</u> 0.11-0.14 mg cm^{-2} d^{-1} 0.05 mg cm^{-2} d^{-1} <u>In karst source stream:</u> 0.005 mg cm^{-2} d^{-1} <u>Total:</u> 0.23-4.4 g yr^{-1}

Yokoyama and Matsukara (2006)	Granodiorite	__	In and above an aquifer, over ten years	Weight loss - percentage	0.013 wt% yr^{-1} above the aquifer, 0.42 wt% yr^{-1} in the aquifer
Krklec et al. (2024)	Limestone	Mean annual temp 4.7°C	In an open slope, small clearing, and bottom of a doline, not in a river channel, precipitation based	Average weathering rate (%)	0.149, 0.160, 0.502% (in each position, same order as the previous column)
Cahoon et al. (1993)	Micritic Limestone	__	In a creek mouth versus by the limestone wall in the lake the creek runs into, over 108 days	Mass loss percentage and average rate	<u>In the creek mouth:</u> 9.59% (6.37 g yr^{-1}) <u>In the lake:</u> 3.56% (2.29 g yr^{-1})

Due to the timeframe of the project, the scope of the field cube research may not be fully representative. In a country with clear seasonality of precipitation patterns (like in the UK), mass loss rates from the spring, especially a dry spring like the Northeast of England had this study period year, may not be fully representative of rates that would occur at different times of year. As such, 120 days is shorter than many field studies using tablets have been in the past (Table 3). A longer-term study looking at cubes at these positions in Trout Beck would be useful to extend on the data found and see if the average mass loss rates is consistent over time, or whether some kind of seasonality exists. Additionally, the cubes may take time to develop a weathering skin, which may then cause a change in weathering rates after this preparatory phase. The cubes have been placed back into the same positions, so this dataset will be grown over the next year to see how these rates may change. As the mass losses measured from the 120-day dataset were all under 4 g, and on average under 0.75 g, longer-term monitoring will be crucial to see if these small reported losses were from erosional processes or from handling and weighing errors.

In summary, the most statistically significant control on dissolution rates that was found through either laboratory or field work was the pH of the solution. The laboratory results gave a clear result in which there was a statistically significant difference between mass loss at pHs 3 and 5, and 3 and 7, with a logarithmic regression showing that pH was a statistically significant predictor of mass loss. While this was not tested directly in the field, low pH run off from the peat bogs that had direct contact with the bench cubes, and only diluted contact with the pool ones, could have been the cause of the higher mass loss of the bench cubes. Temperature did not have a statistically significant control on mass loss at the temperature range tested. While the temperature range tested was lower than many past laboratory experiments looking at dissolution rates, it matched the range at the UK based field site, showing results that are more closely linked to fluvial processes than many in the past which were performed for engineering purposes (Table 2). The field results were more inconclusive, as there was less control over the factors being looked at. Additionally, the low mass losses leave a large level of uncertainty, as potential issues with weighing and handling might make up a larger proportion of the mass lost. The exact influence of immersion time, versus wetting and drying, temperature, and pH that the different cube sets were exposed to cannot be quantified.

8.2 How does rock composition affect carbonate bedrock dissolution rates in a laboratory setting?

In the mill experiments, the relative calcium content of the concrete rock disk correlated with the proportion of mass loss that occurred due to dissolution (Figure 19). The disk with the lowest calcium content (at 251,177.1 ± 2,087.25 ppm) had the lowest proportion of dissolved mass loss, at 58%, in the run with pH 3 and beads. This was even lower than the abrasion only control pH 7 runs with beads on a

1[ce]:1[sa]:1[sh] disk. The intermediate calcium content, found in the 1[ce]:1[sa]:1[sh] disk (260,890 ± 2,204.06ppm) had 85.76% of its mass loss occur through dissolved mass loss. The highest calcium content, in the 1[ce]:2[sh] disk with a calcium content of 345,732.75 ± 2,718.82 ppm had the highest dissolved loss, almost as much as the 1[ce]:1[sa]:1[sh] with pH 3 and no beads, at 93.67%. While calcium content appears to influence the proportion of mass loss that occurs through dissolution versus abrasion, it is not a control on the overall mass loss. The least calcium rich disk (the 1[ce]:2[sa] disk) lost more mass overall than the other disks (Figure 19). While this disk lost the least mass due to dissolution proportionally (only 58%), in grams it lost nearly as much mass as the 1[ce]:2[sh] disk due to dissolution (8.28 vs 8.50 g). While more calcium content means more potential dissolution loss of mass, the texture due to grain size distribution of the materials that make up the disk, as well as the tensile strength, impacts the reaction rates through more rapid exposure of calcium on the fresh bed surface.

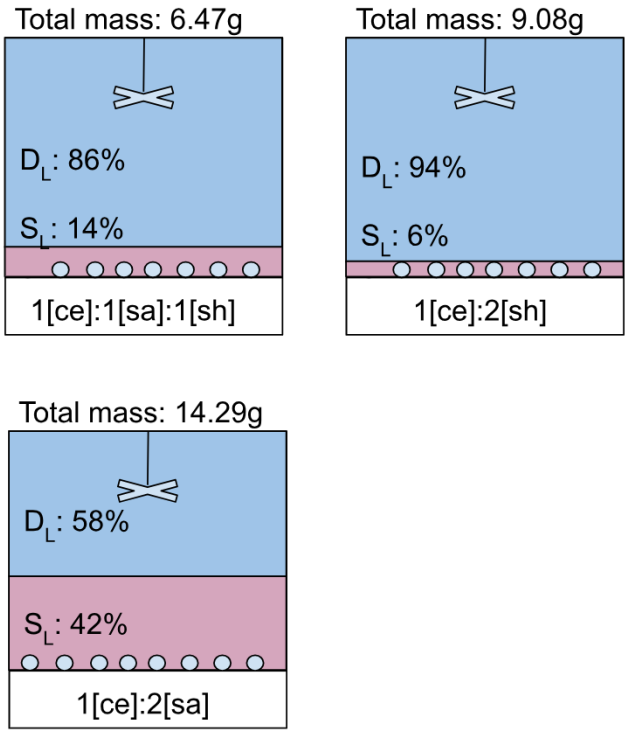

Figure 19: Diagram showing the proportion of total mass loss that occurred through dissolved load (D_L) and suspended load (S_L) in abrasion mill experiments run at pH 3, with abrasive beads, for 35 hours

The 1[ce]:2[sh] and 1[ce]:2[sa] disks both had the same proportion of cement, which has a grain size of roughly 1-50 µm (Zoz et al., 2004). However, the grain size distributions of the sand and shell making up the remaining two thirds were different. The sand had 80% of its mass falling between 195 and 485 µm, with a D_{50} of 308 µm while the shell material had a larger grain size distribution, with 80% between 500

μm and 2 mm, and a D_{50} of 500 μm (Figure 9). The shell material's grain size distribution had to be performed by hand, in stacking sieves, as the particle size analyser could not read the grain size, as the vibration of the solution necessary to agitate the particles continually broke the shell down into pieces, preventing the lasers from getting a clear reading. There is a potential that the mixing process for the concrete would have similarly agitated and broken down some of the shell material, resulting in a finer grain size and narrower grain size distribution being set in the cement-shell mixture. Grain sizes as well as grain shape have been shown to control the tensile strength of cured concrete (Faramarzi and Rezaee, 2018). Larger grains result in stronger cured concrete, while increased length-to-diameter ratio in the components of concrete led to a decrease in tensile strength (Faramarzi and Rezaee, 2018). In bedrock, the grain size composition of the minerals has also been shown to directly influence bedrock abrasion rates. Larger mineral grain sizes, as well as more irregularly shaped fragments, can be more difficult to pivot out of the bedrock surface in order to remove and entrain, meaning that coarser grained lithologies can be more resistant than finer grained lithologies to abrasion (Larimer et al., 2022). These two disks had tensile strength measurements of 2.10±0.20 for the 1[ce]:2[sa] combination and 3.8±0.55 for the 1[ce]:2[sh] disk. This could have contributed to the lower overall erosion rates, and suspended mass loss totals, seen in the shell-dominant disk. Additionally, as the sand could not undergo dissolution, it could have been entrained and acted as an additional abrasive material, furthering suspended load rates in the 1[ce]:2[sa] runs, while the carbonate shell components would dissolve before being entrained.

The effect of surface area available on dissolution rates was tested in the cube experiments. When measured in grams, grams per centimeter-squared, or in percent mass loss there was no difference in mass loss across the cubes of size 3, 4, and 5 cm edge length at pH 3, 17°C, but that there was a linear correlation between percent mass loss and g cm^{-2}, with lower loss explained by higher cube edge lengths. As the experiments did not have a flow through mechanism, and mass loss has been shown above to be pH driven, it is possible that the larger cubes lost the same mass as the smaller ones as the maximum mass lost is controlled by the amount of dissolution that saturates 900 mL of pH 3 solution. This would then suggest that if there was a flow through element in which the acidity was being refreshed, the larger cubes would lose more as there is more fresh material to be dissolved. However, pH logging was not performed on these cube experiments, so the buffer times were not tracked. In the future, experiments should be done comparing surface area in laboratory simulation like these, but either with buffer times tracked or with a flow through mechanism, so that more representative dissolution rates can be tracked and quantified. However, the ability of the solution to completely buffer at every size of cube suggests as calcite is dissolved from the cube surface, the unsaturated solution can continue acting on freshly exposed calcite that was below the initial surface layer.

8.3 What are the relative contributions of physical and chemical processes to overall erosion rates of carbonate bedrock in laboratory experiments?

The mill experiments on the 1[ce]:1[sa]:1[sh] disks showed that both chemical and physical erosive processes can cause high rates of mass loss on carbonate bedrock (Figure 20). The abrasion mill experiments with chemical dissolution only (pH 3, no beads) and physical abrasion only (pH 7, beads) caused 3.64 and 3.05 g of total mass loss, respectively. This shows that at the extreme limits, where either abrasive material is maximized, or the solution is at the lowest pH (pH 3), the rates of chemical and physical erosion are very similar. When both chemical and physical erosional processes are combined, an average of 6.47 g of mass loss occurred (5.20 g and 7.74 g), which is very similar to the combined mass of the two independent processes. In every experimental run, dissolved load was the dominant component of mass loss, with the majority of mass loss not accounted for in the suspended load. The lowest proportion of dissolved load in any run was 70%, still accounting for well over half of the mass loss.

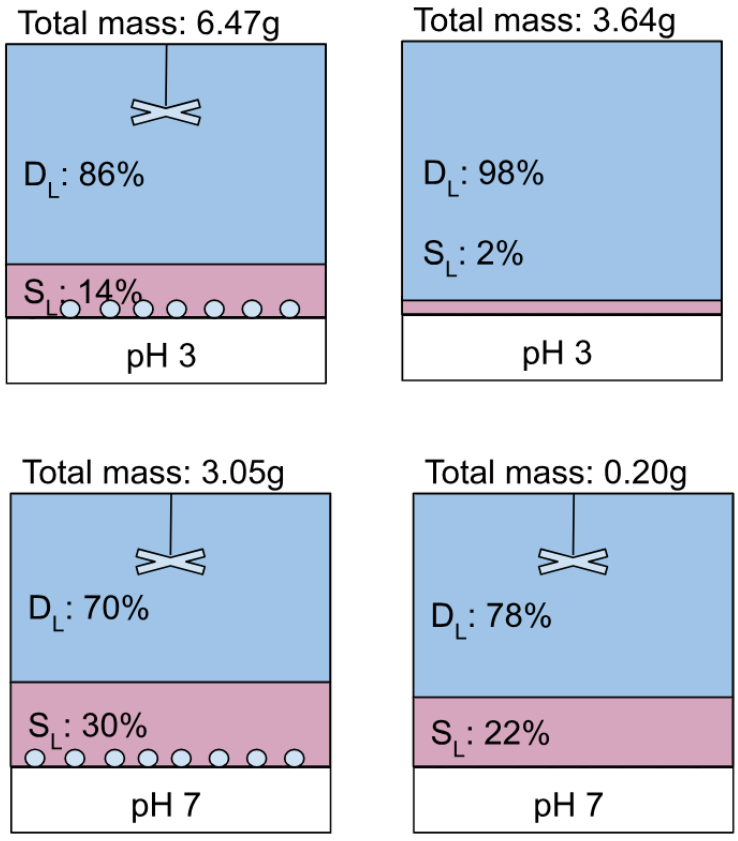

Figure 20: Diagram showing the proportion of total mass loss that occurred through dissolved load (D_L) and suspended load (S_L) in abrasion mill experiments run at pH 3 and pH 7, each with and without

abrasive beads, for 35 hours. All the disks are 1[ce]:1[sa]:1[sh]. pH 3 with beads was run for two sets of 35 hours, the average of these two runs is shown in this diagram.

The control run with neutral solution (filled with deionised water), and no abrasive material still caused 0.20 g of mass loss. As the mill was not a closed system, the deionised water could draw CO2 from the atmosphere to acidify through the creation of carbonic acid (Equation 5). Therefore, the pH 7 run with beads is likely to have dissolution occurring as well, as seen through the proportion of the mass loss that was not caught by the filtering.

$$CO_2(aq) + H_2O \leftrightarrow H_2CO_3 \leftrightarrow HCO_3 + H^+ \leftrightarrow CO_3^{2-} + 2H^+$$

Equation 5: The carbonate buffer system that occurs when carbon dioxide (CO_2) dissolves in water (H_2O)

Table 18 shows the mass loss rates of the field cube positions (averaged across the limestone cubes at each position), the mill rates at each combination of pH and abrasive load, and averaged cube mass losses at each pH or temperature band. Even in the mill control run at pH 7 with no beads, the mass loss rates in g day^{-1} are all at least an order of magnitude larger than the highest of the field rates, found in the bench cubes, although the field cubes had 1.72 times more calcium than the 1[ce]:1[sa]:1[sh] disk used for the experimental runs in Table 18. The mill shows an idealistic version of both erosive processes (abrasion and dissolution) – the abrasive load was chosen to strike the balance of cover and tools effect, while the pH was topped up to ensure that the pH3 runs did not reach a neutral pH. The field cubes likely underwent both dissolution and abrasion, as well as fatigue from wetting-drying cycles, but these processes were more intermittent than in the abrasion mill. Mass loss rates for the field calculated as total mass loss divided by actual time of immersion are closer to those from the mill (Table 18). When normalizing by immersion/inundation time, the bench cubes have undergone about three times the mass loss in a day as was recorded for the mill control run (neutral pH, no beads), but still an order of magnitude less than the other combinations of beads and pH, suggesting a mixture of physical processes (likely wetting-drying cycles) and dissolution drove mass loss in the field cube experiments, but at much lower rates that were produced in the abrasion mill.

Table 18: Averaged mass loss rates found in the abrasion mill, laboratory cubes, and field experiments ran (starred value shows the mass loss rate normalised for immersion time)

Experiment	**Lithology**	**Averaged mass loss rate (g d^{-1})**
Field pool cubes	Limestone	0.01
Field bench cubes	Limestone	0.01 | 0.39*
Field atmosphere cubes	Limestone	< 0.01
Mill pH 7 with no beads	Concrete: 1[ce]:1[sa]:1[sh]	0.13
Mill pH 7, with beads	Concrete: 1[ce]:1[sa]:1[sh]	2.09
Mill pH 3 with no beads	Concrete: 1[ce]:1[sa]:1[sh]	2.50
Mill pH 3, with beads	Concrete: 1[ce]:1[sa]:1[sh]	4.44
Cubes at pH 3	Limestone	0.26
Cubes at pH 5	Limestone	0.04
Cubes at pH 7	Limestone	0.03
Cubes at 3°C	Limestone	0.10
Cubes at 17°C	Limestone	0.12
Cubes at 30°C	Limestone	0.11

The higher rates of mass loss found in the mill experiments could also be due to the differences between natural limestone (as used in the cube experiments) and the concrete used in the mill. The mill experiments were solely performed on calcium-rich concrete, acting as a stand-in for limestone bedrock lithologies. Even the 1[ce]:2[sh] disk, which had the highest calcium concentration of the three disk compositions (345,733 ± 2,719) had less calcium than the limestone blocks used in both sets of cube experiments, cut from the field site (448,170 - 448,544 ppm ±2193-3206). This means the proportion of mass loss due to dissolution for the natural limestone would likely be higher than what was found for the concrete used in the mill experiments. Natural limestone generally has a higher tensile strength than that found for the concrete used, so overall rates of mass loss from the combined processes in the mill would likely occur at a slower rate (Figure 21).

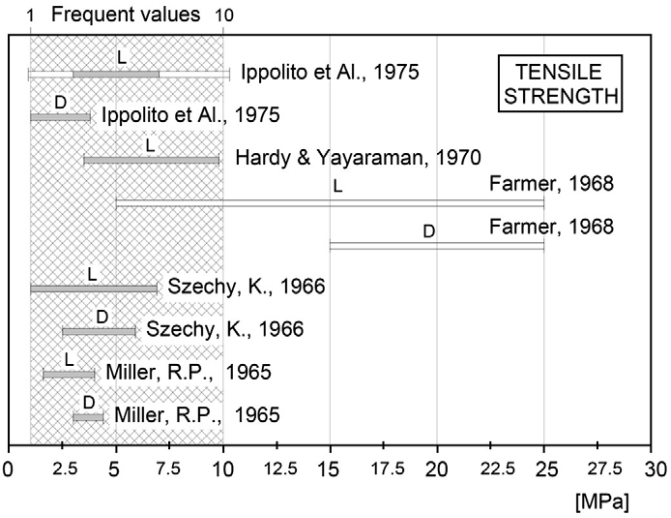

Figure 21: The characteristic values of tensile strength for limestone and dolomitic rocks (Paronuzzi and Serafini, 2009)

This thesis has critically analysed how physical and chemical erosive processes can potentially enhance rates of the other, through the addition of either acidic solution, or abrasive tools. These experiments found evidence that the addition of abrasive tools, at each pH, led to a large increase in dissolved mass loss (~14 times (2g) at pH 7, and 1.57 times (2.03 g) at pH 3). The addition of acidic solution did not cause a discernable increase in suspended mass loss in the runs with abrasive tools. This supports previous work (Cahoon et al., 1993; Hoch and Drever, 1999; Dabski et al., 2019) that theorized that physical weathering of limestone increased chemical weathering rates, as it increased the exposed surface area available to be chemically attacked through changing the surface's roughness. It was also hypothesized that higher rates of chemical weathering would lead to more abrasion, but this was not found in the mill experiments. It was expected that if more of the dissolvable minerals were dissolved, then the surrounding non-dissolvable sand grains would be more prone to release as suspended load. This did not occur, potentially as the cementation process meant that the sand was more bonded to the disk, meaning more mass loss by dissolution needed to occur for them to be entrained.

In the field, the limestone cubes lost more mass than the sandstone ones at both positions that included immersion – the pool and bench (1.08 g vs 0.55 g and 1.56 g vs 0.25 g, respectively). This is likely due to dissolution, which would affect the limestone more, as it is composed primarily of calcium carbonate, a compound prone to chemical dissolution. Sandstone is composed of quartz minerals cemented together by primarily silica, calcite (the mineral form of calcium carbonate), clay or iron oxide (Beck and Crook, 2025). Of these materials, calcite is easily attacked by chemical dissolution, but sandstone has a lower calcium component than limestone, so is less prone to chemical weathering. However, the strength and

composition of the cubes would likely have an impact on the mass loss of these different lithologies. Sandstone has been shown to be mechanically weaker and less resistant to abrasion – experiments run with abrasion mills found that sandstone took an average of 14.1 hours to have 5-10 g of mass loss, whereas limestone took an average of 49.3 hours (Turowski et al., 2023). This suggests that if the mass loss was abrasion driven, the sandstone cubes in the field would have lost more mass than the limestone ones. As the reverse is true, it is likely that a large proportion of the mass loss is due to dissolution, or wetting-drying cycles rather than abrasion.

8.4 Wider implications and future research

Through examining the effects of dissolution and abrasion on carbonate mass loss, in the field and laboratory, this study provides compelling evidence that chemical dissolution is an important process in fluvial systems, necessitating the need for further research. The results of both the cube and mill experiments showed that even in near-neutral pH environments, there is potential for dissolution to occur, perhaps through carbon drawdown causing the creation of carbonic acid (Equations 1 and 2). pH was found to be the main control on dissolution rate, with temperature showing no statistical significance over mass loss.

Understanding the effects that different factors such as pH, temperature, carbon cycling, and immersion time have on fluvial bedrock erosion is especially crucial for mitigation plans relating to future climate change. Shifting chemical weathering pathways could become a major control in bedrock river dissolution, as these pathways could impact pH. As climate change continues to change vegetation coverage and precipitation patterns on Earth, knock on effects through changing runoff regimes could have a further effect on the pH of fluvial systems (Heijmans et al., 2008; Chalchissa and Kuris, 2024). Sulfide weathering, and other anthropogenic acidity sources from industry and agricultural fertilizer regimes could grow as core causes of acidity in river systems globally (Raymond et al., 2012; Guo et al., 2015). Rising temperatures may also bring river system water temperatures higher, into ranges above those tested in this study that may enact more control on dissolution rates (Alkattan et al., 1998; Kabir et al., 2023). Additionally, rising temperatures mean more river systems will shift away from near freezing temperature regimes, which buffering patterns suggested may have lower dissolution rates than systems at higher temperatures (Figure 12). As carbonate landforms are one of the biggest carbon sinks in the world, the release of carbon from the dissolution of calcium (Equations 2 and 3) could further contribute to the issue of rising CO_2 levels, potentially creating a positive feedback loop with temperatures rising. Changing precipitation and storm patterns will also change immersion rates through modifying discharge, which then changes hydraulic properties as well as dissolution regimes. Knowledge of how fluvial

systems act, and therefore how they may respond to future changes, can inform environmental models, ensuring a more holistic view on how the planet runs, and will run.

Further studies could perform more runs of the cube experiments at each pH and temperature combinations, cutting the run time to equal the buffer time, or flow-through technology could be used to more consistently re-acidify the solution. Similarly, more acid could be added during predefined intervals relating to buffering time in the cube experiments, so that the pH stayed closer to the initial pH through a larger portion of the run. This could also be done for the cube size comparison experiments, to see whether the lack of difference in mass loss as measured in grams was due to inhibition from the amount of HCl available for dissolution chemical processes, or whether the cube size does not have an effect. Additionally, the cube experiments could be run at more incremental pHs between 3 and 5 to determine where the threshold is where dissolution rates accelerate.

For the abrasion mill experiments, more experiments at each combination would be helpful to reiterate results and see if slight differences in runs of the same combination of pH and abraders eventually even out to a steady mean. The abrasion mill could also be run at different pHs. Runs using pH 5 solution were not conducted based on the observation that there was no difference in mass loss for pH 5 and pH 7 cube experiment runs. It would be beneficial to see if the addition of abrasive tools meant that a difference between pH 5 and pH 7 related mass loss did emerge. In addition, running experiments with bedrock disks from the field site would further standardize results, making the abrasion mill results more directly comparable with the field and laboratory cube results. To isolate the effects of constituent grain size on the abrasion mill experiment, similar grain sized sand and shell mixtures could be used. This would allow the effect of calcium content on dissolution rates to be more directly compared.

9. Conclusion

This study provides one of the first assessments of the comparative rates and magnitudes of chemical weathering and physical erosion in a limestone bedrock river setting. This was completed through the use of a combined field and laboratory work approach. Overall, the results suggest that chemical weathering has been previously underestimated in fluvial systems and has the potential to contribute similar rates and magnitudes of mass removal as physical erosion.

Laboratory experiments, building on past abrasion mill research, were used to study a combination of abrasion and chemical dissolution, and showed that when viewed in isolation abrasion or chemical dissolution (from pH 3 solution), resulted in similar rates of erosion 2.09 and 2.50 grams per day, respectively. When both chemical and physical erosional processes were combined (in the pH 3 with beads runs), an average of 6.47 g of mass loss occurred. These experiments also found evidence that the presence of physical erosion increased the rates of dissolution (at both pH 3 and 7), while the addition of acid into runs with abrasive bead load did not cause an increase in suspended mass loss.

Laboratory experiments comparing chemical dissolution rates of limestone cubes at different pH (3, 5, 7) and temperature (3°, 17°, 30°) combinations showed that changes in pH of the solution was a statistically significant predictor of mass loss variation. However, there was no statistically significant difference in mass loss between cubes that were suspended in pH 5 and pH 7 solutions, showing that the relationship likely includes a rapid increase in dissolution at a pH between 5 and 3. Temperature was not shown to be a significant control over dissolution rates in the cube dissolution experiments. However, it took a statistically longer time for the solution to buffer from pH 3 to 7 at the coldest temperature, while there was no statistical difference between the two higher temperatures (17° and 30°C), again suggesting that there may be a threshold response where dissolution rates significantly increase after a certain temperature between 3 and 17°C. This can be tested in the future through a flow through mechanism, in which the pH 3 solution is stabilised through constant acid influx, allowing for more accurate rates of mass loss to be attained.

In the field, wetting-drying cycles were inferenced to be a driving factor of mass loss in limestone cubes fixed at different positions within the river channel. Although there was no statistical difference between the average mass loss of cubes suspended on the river bench (which were inundated 4 of 120 days) versus those in the river pool (inundated 120 of 120 days), the average mass loss on the bench was 1.4x that of the cubes in the pool. As the pool cubes were immersed for 30 times as long as the bench cubes were, it was hypothesized that they would lose more mass. This discrepancy was likely because mass loss from

wetting-drying cycles, causing stress and eventual breakdown, was more significant than originally assumed. Additionally, low pH runoff from the peat would be less diluted when interacting with the bench cubes than the pool ones.

The calcium content of concrete disks used in an abrasion mill controlled the rates of chemical dissolution when both chemical weathering (pH 3 solution) and abrasion (borosilicate bead abraders) were present. The three disk compositions tested had proportions of suspended versus dissolved mass loss that correlated with their relative calcium contents to each other. However, the overall mass loss of the disks did not align with their calcium contents, and the least calcium risk disk almost had as much mass loss due to dissolution as the most calcium rich one due to its overall larger mass loss. This was also because physical abrasion was found to increase chemical weathering more than chemical weathering raised rates of physical erosion, meaning that the tensile strength of the disks, and thus their susceptibility to abrasion, was an important factor in dissolution rates as well.

The evidence that this study provides on the importance of chemical weathering in fluvial systems is crucial in order to reframe the current paradigm that places chemical dissolution as negligible in models that incorporate fluvial systems. As the climate continues to change, and with it the controls on chemical weathering that this study interrogated, building knowledge on how important these controls are, and how the balance in relative importance may shift in the future is key in creating strong plans to mitigate the future of Earth.

10. References

Alkattan, M., Oelkers, E.H., Dandurand, J.L. and Schott, J., 1998. An experimental study of calcite and limestone dissolution rates as a function of pH from− 1 to 3 and temperature from 25 to 80 C. *Chemical geology*, *151*(1-4), pp.199-214.

Al-Bared, A.M., Harahap, I.S.H., Azuddin, N.H., Marto, A., Abad, S.A.N.K., Ali, M.O.A. and Isah, B.W., 2020, April. Degradation of limestone exposed to drying and wetting cycles–experimental study. In *IOP Conference Series: Earth and Environmental Science* (Vol. 476, No. 1, p. 012040). IOP Publishing.

Banas, K. and Gos, K., 2004. Effect of peat-bog reclamation on the physico-chemical characteristics of the ground water in peat. *Polish Journal of Ecology*, *52*(1), pp.69-74.

Beck, K. C., & Crook, K. A. W. (2025). *Sedimentary rock types*. Encyclopædia Britannica. https://www.britannica.com/science/sedimentary-rock/Sandstones

Beer, A.R. and Lamb, M.P., 2021. Abrasion regimes in fluvial bedrock incision. *Geology*, *49*(6), pp.682-386.

Briolet, T., Bemer, E., Sissmann, O. and Fortin, J., 2025. Localized versus distributed dissolution in carbonate rocks: The key role of microstructure. *Geochimica et Cosmochimica Acta*, *397*, pp.113-133.

Beer, A.R. and Turowski, J.M., 2015. Bedload transport controls bedrock erosion under sediment-starved conditions. *Earth Surface Dynamics*, *3*(3), pp.291-309.

Brake, S., Connors, K. and Romberger, S., 2001. A river runs through it: impact of acid mine drainage on the geochemistry of West Little Sugar Creek pre-and post-reclamation at the Green Valley coal mine, Indiana, USA. *Environmental Geology*, *40*(11), pp.1471-1481.

Cahoon, L.B., Kucklick, J.R., Kiefer, R.H. and Willey, J.D., 1993. The Effects of Chemical Weathering on Limestone Dissolution and Phosphate Release into Lake Waccamaw, North Carolina. *Journal of the Elisha Mitchell Scientific Society*, pp.123-134.

Campbell, S.W., Dixon, J.C., Darmody, R.G. and Thorn, C.E., 2001. Spatial variation of early season surface water chemistry in Kärkevagge, Swedish Lapland. *Geografiska Annaler: Series A, Physical Geography*, *83*(4), pp.169-178.

Campbell, S.W., Dixon, J.C., Thorn, C.E. and Darmody, R.G., 2002. Chemical denudation rates in Kärkevagge, Swedish Lapland. *Geografiska Annaler: Series A, Physical Geography*, *84*(3-4), pp.179-185.

Chakrapani, G.J., 2005. Factors controlling variations in river sediment loads. *Current science*, pp.569-575.

Chalchissa, F.B. and Kuris, B.K., 2024. Modeling the impacts of extreme climate scenarios on soil acidity (pH and exchangeable aluminum) in Abbay River Basin, Ethiopia. *Heliyon*, *10*(12).

Cook, K.L., Turowski, J.M. and Hovius, N., 2013. A demonstration of the importance of bedload transport for fluvial bedrock erosion and knickpoint propagation. *Earth Surface Processes and Landforms*, *38*(7), pp.683-695.

Covington, M.D., Gulley, J.D. and Gabrovšek, F., 2015. Natural variations in calcite dissolution rates in streams: Controls, implications, and open questions. *Geophysical Research Letters*, *42*(8), pp.2836-2843.

Dąbski, M., Woronko, B., Fabijańska, P. and Otto, J.C., 2019. Micro-weathering of limestone surfaces in a foreland of Hallstätter Glacier (Dachstein, Austria). *Geografiska Annaler: Series A, Physical Geography*, *101*(3), pp.277-292.

Dai, J., Zhang, J., Xu, H., Wang, Y., Zhang, G., Xu, Y. and Hu, X., 2021. Effects of bedrock erosion by tillage on architectures and hydraulic properties of soil and near-surface bedrock. *Science of the Total Environment*, *790*, p.148244.

Darwish, M.M., Fowler, H.J., Blenkinsop, S. and Tye, M.R., 2018. A regional frequency analysis of UK sub-daily extreme precipitation and assessment of their seasonality. *International Journal of Climatology*, *38*(13), pp.4758-4776.

Davy, P. and Lague, D., 2009. Fluvial erosion/transport equation of landscape evolution models revisited. *Journal of Geophysical Research: Earth Surface*, *114*(F3).

Deal, E., Braun, J. and Botter, G., 2018. Understanding the role of rainfall and hydrology in determining fluvial erosion efficiency. *Journal of Geophysical Research: Earth Surface*, *123*(4), pp.744-778.

Dingle, E.H., Baynes, E.R., Hall, A. and Warburton, J., 2025. Erosion dynamics in carbonate bedrock channels inhibit weathering processes. *Earth Surface Processes and Landforms*, *50*(5), p.e70067.

Dong, W., Li, Z., Shen, L., Liu, W., Guo, Y., Xu, H. and Yong, R., 2024. Study on the process of mass transfer and deterioration of limestone under dynamic dissolution of CO2 solution. *Scientific Reports*, *14*(1), p.5278.

Dubinski, I.M. and Wohl, E., 2013. Relationships between block quarrying, bed shear stress, and stream power: A physical model of block quarrying of a jointed bedrock channel. *Geomorphology*, *180*, pp.66-81.

Emmanuel, S. and Levenson, Y., 2014. Limestone weathering rates accelerated by micron-scale grain detachment. *Geology*, *42*(9), pp.751-754.

Faramarzi, L. and Rezaee, H., 2018. Testing the effects of sample and grain sizes on mechanical properties of concrete. *Journal of Materials in Civil Engineering*, *30*(5), p.04018065.

Finnegan, N.J., Sklar, L.S. and Fuller, T.K., 2007. Interplay of sediment supply, river incision, and channel morphology revealed by the transient evolution of an experimental bedrock channel. *Journal of Geophysical Research: Earth Surface*, *112*(F3).

Frei, M., Bielert, U. and Heinrichs, H., 2000. Effects of pH, alkalinity and bedrock chemistry on metal concentrations of springs in an acidified catchment (Ecker Dam, Harz Mountains, FRG). *Chemical Geology*, *170*(1-4), pp.221-242.

Gaillardet, J., Calmels, D., Romero-Mujalli, G., Zakharova, E. and Hartmann, J., 2019. Global climate control on carbonate weathering intensity. *Chemical Geology*, *527*, p.118762.

Gregory, K.J., 2010. *The Earth's land surface: landforms and processes in geomorphology*. Sage Publications.

Gu, D., Liu, H., Gao, X., Huang, D. and Zhang, W., 2021. Influence of cyclic wetting–drying on the shear strength of limestone with a soft interlayer. *Rock Mechanics and Rock Engineering*, *54*(8), pp.4369-4378.

Gundersen, P. and Steinnes, E., 2001. Influence of temporal variations in river discharge, pH, alkalinity and Ca on the speciation and concentration of heavy metals in some mining polluted rivers. *Aquatic geochemistry*, *7*(3), pp.173-193.

Guo, J., Wang, F., Vogt, R.D., Zhang, Y. and Liu, C.Q., 2015. Anthropogenically enhanced chemical weathering and carbon evasion in the Yangtze Basin. *Scientific reports*, *5*(1), p.11941.

Han, G., Tang, Y. and Xu, Z., 2010. Fluvial geochemistry of rivers draining karst terrain in Southwest China. *Journal of Asian Earth Sciences*, *38*(1-2), pp.65-75.

Hattanji, T. and Matsukura, Y., 2017. Factors controlling weathering rates of carbonate rocks in soil: An approach from a field weathering experiment. *JOURNAL OF GEOGRAPHY-CHIGAKU ZASSHI*, *126*(3), pp.355-367.

Hattanji, T., Ueda, M., Song, W., Ishii, N., Hayakawa, Y.S., Takaya, Y. and Matsukura, Y., 2014. Field and laboratory experiments on high dissolution rates of limestone in stream flow. *Geomorphology*, *204*, pp.485-492.

Heijmans, M.M., Mauquoy, D., Van Geel, B. and Berendse, F., 2008. Long-term effects of climate change on vegetation and carbon dynamics in peat bogs. *Journal of Vegetation Science*, *19*(3), pp.307-320.

Hoch, A.R., Reddy, M.M. and Drever, J.I., 1999. Importance of mechanical disaggregation in chemical weathering in a cold alpine environment, San Juan Mountains, Colorado. *Geological Society of America Bulletin*, *111*(2), pp.304-314.

Hodson, A., Heaton, T., Langford, H. and Newsham, K., 2010. Chemical weathering and solute export by meltwater in a maritime Antarctic glacier basin. *Biogeochemistry*, *98*, pp.9-27.

Howard, A.D., Dietrich, W.E. and Seidl, M.A., 1994. Modeling fluvial erosion on regional to continental scales. *Journal of Geophysical Research: Solid Earth*, *99*(B7), pp.13971-13986.

Johnson, G.A.L., 1963. *The geology of Moor House: a national nature reserve in north-east Westmorland* (No. 2). HM Stationery Office.

Kabir, M., Habiba, U.E., Khan, W., Shah, A., Rahim, S., De los Rios-Escalante, P.R., Farooqi, Z.U.R., Ali, L. and Shafiq, M., 2023. Climate change due to increasing concentration of carbon dioxide and its impacts on environment in 21st century; a mini review. *Journal of King Saud University-Science*, *35*(5), p.102693.

Knighton, D., 1998. *Fluvial forms and processes: a new perspective*. Routledge.

Kohitlhetse, I., Thubakgale, K., Mendonidis, P. and Manono, M., 2021. Investigating the effect of reaction temperature on the extraction of calcium from ironmaking slag: A kinetics study. *Environmental Sciences Proceedings*, *6*(1), p.31.

Krklec, K., Bočić, N., Perica, D. and Domínguez-Villar, D., 2024. Investigation of short-term denudation rates using the rock tablet method in Northern Velebit National Park (Croatia). *Croatian Geographical/Hrvatski Geografski Glasnik*, *86*(1).

Lague, D., Hovius, N. and Davy, P., 2005. Discharge, discharge variability, and the bedrock channel profile. *Journal of Geophysical Research: Earth Surface*, *110*(F4).

Lamarca-Irisarri, D., Van Driessche, A.E., Jordan, G., Cappelli, C. and Huertas, F.J., 2019. The role of pH, temperature, and NH4+ during mica weathering. *ACS Earth and Space Chemistry*, *3*(11), pp.2613-2622.

Lamb, M.P., Finnegan, N.J., Scheingross, J.S. and Sklar, L.S., 2015. New insights into the mechanics of fluvial bedrock erosion through flume experiments and theory. *Geomorphology*, *244*, pp.33-55.

Larimer, J.E., Yanites, B.J. and Jung, S.J., 2022. A field study on the lithological influence on the interaction between weathering and abrasion processes in bedrock rivers. *Journal of Geophysical Research: Earth Surface*, *127*(4), p.e2021JF006418.

Leng, P., Li, F., Du, K., Li, Z., Gu, C. and Koschorreck, M., 2020. Flow velocity and nutrients affect CO2 emissions from agricultural drainage channels in the North China Plain. *Environmental Sciences Europe*, *32*(1), p.146.

Li, T., Fuller, T.K., Sklar, L.S., Gran, K.B. and Venditti, J.G., 2020. A mechanistic model for lateral erosion of bedrock channel banks by bedload particle impacts. *Journal of Geophysical Research: Earth Surface*, *125*(6), p.e2019JF005509.

Li, H., Wang, S., Bai, X., Cao, Y. and Wu, L., 2019. Spatiotemporal evolution of carbon sequestration of limestone weathering in China. *Science China Earth Sciences*, *62*, pp.974-991.

Liu, Z. and Dreybrod, W., 1997. Dissolution kinetics of calcium carbonate minerals in H2O CO2 solutions in turbulent flow: The role of the diffusion boundary layer and the slow reaction H2O+ CO2→ H++ HCO3−. *Geochimica et cosmochimica acta*, *61*(14), pp.2879-2889.

Macpherson, G.L., Roberts, J.A., Blair, J.M., Townsend, M.A., Fowle, D.A. and Beisner, K.R., 2008. Increasing shallow groundwater CO2 and limestone weathering, Konza Prairie, USA. *Geochimica et Cosmochimica Acta*, *72*(23), pp.5581-5599.

Marra, K.R., Madden, M.E.E., Soreghan, G.S. and Hall, B.L., 2017. Chemical weathering trends in fine-grained ephemeral stream sediments of the McMurdo Dry Valleys, Antarctica. *Geomorphology*, *281*, pp.13-30.

Matsubara, H., Morimoto, S., Sase, H., Ohizumi, T., Sumida, H., Nakata, M. and Ueda, H., 2009. Long-term declining trends in river water pH in central Japan. *Water, air, and soil pollution*, *200*(1), pp.253-265.

Meybeck, M., 1987. Global chemical weathering of surficial rocks estimated from river dissolved loads. *American journal of science*, *287*(5), pp.401-428.

Murphy, B.P., Johnson, J.P., Gasparini, N.M. and Sklar, L.S., 2016. Chemical weathering as a mechanism for the climatic control of bedrock river incision. *Nature*, *532*(7598), pp.223-227.

Oelkers, E.H. and Helgeson, H.C., 1988. Calculation of the thermodynamic and transport properties of aqueous species at high pressures and temperatures: Aqueous tracer diffusion coefficients of ions to 1000 C and 5 kb. *Geochimica et Cosmochimica Acta*, *52*(1), pp.63-85.

Ohta, A. and Minami, M., 2013. Less impact of limestone bedrock on elemental concentrations in stream sediments–Case study of Akiyoshi area–. *Bulletin of the Geological Survey of Japan*, *64*(5/6), pp.121-138.

Olías, M., Nieto, J.M., Sarmiento, A.M., Cerón, J.C. and Cánovas, C.R., 2004. Seasonal water quality variations in a river affected by acid mine drainage: the Odiel River (South West Spain). *Science of the total environment*, *333*(1-3), pp.267-281.

Panigrahy, B.K. and Raymahashay, B.C., 2005. River water quality in weathered limestone: a case study in upper Mahanadi basin, India. *Journal of earth system science*, *114*, pp.533-543.

Paronuzzi, P. and Serafini, W., 2009. Stress state analysis of a collapsed overhanging rock slab: a case study. *Engineering Geology*, *108*(1-2), pp.65-75.

Rapp, A., 1960. Recent development of mountain slopes in Kärkevagge and surroundings, northern Scandinavia. *Geografiska Annaler*, *42*(2-3), pp.65-200.

Raymond, P.A., David, M.B. and Saiers, J.E., 2012. The impact of fertilization and hydrology on nitrate fluxes from Mississippi watersheds. *Current Opinion in Environmental Sustainability*, *4*(2), pp.212-218.

Rennie, S., Adamson, J., Anderson, R., Andrews, C., Bater, J., Bayfield, N., Beaton, K., Beaumont, D., Benham, S., Bowmaker, V., Britt, C., Brooker, R., Brooks, D., Brunt, J., Common, G., Cooper, R., Corbett, S., Critchley, N., Dennis, P., Dick, J., Dodd, B., Dodd, N., Donovan, N., Easter, J., Flexen, M., Gardiner, A., Hamilton, D., Hargreaves, P., Hatton-Ellis, M., Howe, M., Kahl, J., Lane, M., Langan, S., Lloyd, D., McCarney, B., McElarney, Y., McKenna, C., McMillan, S., Milne, F., Milne, L., Morecroft, M., Murphy, M., Nelson, A., Nicholson, H., Pallett, D., Parry, D., Pearce, I., Pozsgai, G., Rose, R., Schafer, S., Scott, T., Sherrin, L., Shortall, C., Smith, R., Smith, P., Tait, R., Taylor, C., Taylor, M., Thurlow, M., Turner, A., Tyson, K., Watson, H., Whittaker, M., Wood, C. (2017). *UK Environmental Change Network (ECN) stream water chemistry data: 1992-2015. NERC Environmental Information Data Centre. (Dataset).* https://doi.org/10.5285/fd7ca5ef-460a-463c-ad2b-5ad48bb4e22e

Riebe, C.S., Kirchner, J.W. and Finkel, R.C., 2004. Erosional and climatic effects on long-term chemical weathering rates in granitic landscapes spanning diverse climate regimes. *Earth and Planetary Science Letters*, *224*(3-4), pp.547-562.

Rios, S., Viana da Fonseca, A., Consoli, N.C., Floss, M. and Cristelo, N., 2013. Influence of grain size and mineralogy on the porosity/cement ratio. *Géotechnique Letters*, *3*(3), pp.130-136.

Satake, K., Oyagi, A. and Iwao, Y., 1995. Natural acidification of lakes and rivers in Japan: The ecosystem of Lake Usoriko (pH 3.4–3.8). *Water, Air, and Soil Pollution*, *85*(2), pp.511-516.

SHARMA, BISHNU,PRASAD (2016) Sediment Dynamics in a Bedrock Channel, Durham theses, Durham University. Available at Durham E-Theses Online: http://etheses.dur.ac.uk/11942/

Sklar, L.S. and Dietrich, W.E., 2001. Sediment and rock strength controls on river incision into bedrock. *Geology*, *29*(12), pp.1087-1090.

Sklar, L.S. and Dietrich, W.E., 2006. The role of sediment in controlling steady-state bedrock channel slope: Implications of the saltation–abrasion incision model. *Geomorphology*, *82*(1-2), pp.58-83.

Smith, D.I., Greenaway, M.A., Moses, C. and Spate, A.P., 1995. Limestone weathering in eastern Australia. Part 1: Erosion rates. *Earth Surface Processes and Landforms*, *20*(5), pp.451-463.

Spotila, J.A., Moskey, K.A. and Prince, P.S., 2015. Geologic controls on bedrock channel width in large, slowly-eroding catchments: Case study of the New River in eastern North America. *Geomorphology*, *230*, pp.51-63.

Sun, B., Zhou, Q., Xu, T., Hui, S.E. and Shi, Z., 2007. Experimental study on limestone dissolution in acid solution. In *Challenges of Power Engineering and Environment: Proceedings of the International Conference on Power Engineering 2007* (pp. 773-777). Springer Berlin Heidelberg.

Thorn, C.E., Darmody, R.G. and Dixon, J.C., 2011. Rethinking weathering and pedogenesis in alpine periglacial regions: some Scandinavian evidence.

Thorn, C.E., Darmody, R.G., Dixon, J.C. and Schlyter, P., 2001. The chemical weathering regime of Kärkevagge, arctic–alpine Sweden. *Geomorphology*, *41*(1), pp.37-52.

Thornbush, M.J. and Viles, H.A., 2007. Simulation of the dissolution of weathered versus unweathered limestone in carbonic acid solutions of varying strength. *Earth Surface Processes and Landforms: The Journal of the British Geomorphological Research Group*, *32*(6), pp.841-852

Trudgill, S.T. and Viles, H.A., 1998. Field and laboratory approaches to limestone weathering. *Quarterly Journal of Engineering Geology and Hydrogeology*, *31*(4), pp.333-341.

Turowski, J.M., Hovius, N., Meng-Long, H., Lague, D. and Men-Chiang, C., 2008. Distribution of erosion across bedrock channels. *Earth Surface Processes and Landforms: The Journal of the British Geomorphological Research Group*, *33*(3), pp.353-363.

Turowski, J.M., Hovius, N., Wilson, A. and Horng, M.J., 2008. Hydraulic geometry, river sediment and the definition of bedrock channels. *Geomorphology*, *99*(1-4), pp.26-38.

Turowski, J.M., Pruß, G. and Reich, M., 2023a. Experimental Design and Protocol for Standardized Measurements of Rock Erodibility in Fluvial Impact Erosion. *Journal of Hydraulic Engineering*, *149*(12), p.06023010.

Turowski, J.M., Pruß, G., Voigtländer, A., Ludwig, A., Landgraf, A., Kober, F. and Bonnelye, A., 2023b. Geotechnical controls on erodibility in fluvial impact erosion. *Earth Surface Dynamics*, *11*(5), pp.979-994.

Warburton, J. and Evans, M., 2011. Geomorphic, sedimentary, and potential palaeoenvironmental significance of peat blocks in alluvial river systems. *Geomorphology*, *130*(3-4), pp.101-114.

Wasko, C., Nathan, R., Stein, L. and O'Shea, D., 2021. Evidence of shorter more extreme rainfalls and increased flood variability under climate change. *Journal of Hydrology*, *603*, p.126994.

Wohl, E.E., 1998. Bedrock channel morphology in relation to erosional processes. *GEOPHYSICAL MONOGRAPH-AMERICAN GEOPHYSICAL UNION*, *107*, pp.133-152.

Yadav, S.K., Chakrapani, G.J. and Gupta, M.K., 2008. An experimental study of dissolution kinetics of calcite, dolomite, leucogranite and gneiss in buffered solutions at temperature 25 and 5 C. *Environmental geology*, *53*(8), pp.1683-1694.

Yokoyama, T. and Matsukura, Y., 2006. Field and laboratory experiments on weathering rates of granodiorite: separation of chemical and physical processes. *Geology*, *34*(10), pp.809-812.

Zhang, Z., Niu, Y., Shang, X., Ye, P., Zhou, R. and Gao, F., 2021. Deterioration of physical and mechanical properties of rocks by cyclic drying and wetting. *Geofluids*, *2021*(1), p.6661107.

Zoz, H., Jaramillo, D., Tian, Z., Trindade, B., Ren, H., Chimal-V, O. and de la Torre, S.D., 2004. High Performance cements and advanced Ordinary Portland cement manufacturing by HEM-Refinement and activation. *ZKG INTERNATIONAL*, *57*(1), pp.60-70.